PHYSICS
OF
THIN
FILMS

3
1966

Physics of Thin Films

Advances in Research and Development

VOLUME 3

CONTRIBUTORS TO THIS VOLUME

Klaus H. Behrndt

D. E. Bode

L. V. Gregor

R. W. Hoffman

Leon I. Maissel

A. Vecht

Physics of Thin Films

Advances in Research and Development

Edited by

GEORG HASS

Night Vision Laboratory
U. S. Army Electronics Command
Fort Belvoir, Virginia

and

RUDOLF E. THUN

International Business Machines Corporation
Owego, New York

VOLUME 3

1966

ACADEMIC PRESS

NEW YORK AND LONDON
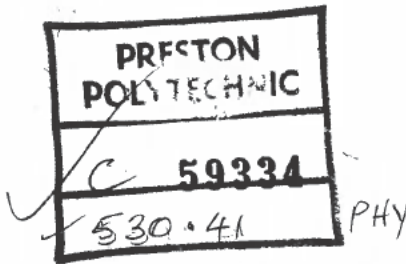
b 6705833

63. A. Rose, "Concepts in Photoconductivity and Allied Problems." Wiley (Interscience), New York, 1963.
64. H. K. Henisch, "Electroluminescence." Pergamon Press, New York, 1962.
65. H. K. Henisch, *Rept. Progr. Phys.* **27**, 369 (1964).
66. H. F. Ivey, Electroluminescence and Related Effects, Suppl. 1, *in* "Advances in Electronics and Electron Physics." Academic Press, New York, 1963.
67. "Photoconductivity" (H. Levinstein, ed.). Pergamon Press, New York, 1961.
68. A. Vecht and B. W. Ely, *Vacuum* **14**, 122 (1964).
69. Y. Sakai and H. Okimura, *Japan. J. Appl. Phys.* **3**, 144 (1964).
70. K. Weiss, *Z. Naturforsch.* **2a**, 650 (1947).
71. J. E. Jacobs and C. W. Hart, *Proc. Nat. Electron. Conf.* **11**, 592 (1955).
72. P. Goercke, *Ann. Telecom.* **6**, 325 (1951).
73. W. Ehrenberg and J. Franks, *Proc. Phys. Soc. (London)* **B66**, 1507 (1953).
74. D. E. N. King, *J. Television Soc.* **10**, 2 (1962).
75. C. Feldman, *J. Soc. Motion Picture Television Engrs.* **67**, 455 (1958).
76. A. Bril, *in* "Luminescence of Organic and Inorganic Materials" (H. P. Kallman and G. M. Spruch, eds.), p. 479. Wiley, New York, 1962.
77. D. A. Cusano, *Pro. Image Intensifer Symp., Fort Belvoir, Va., Oct. 24–26, 1961*, p. 119. *USAEROL*, Fort Belvoir, Virginia.
78. W. A. Thornton, *J. Electrochem. Soc.* **108**, 636 (1961).
79. W. A. Thornton, *Phys. Rev.* **123**, 1583 (1961).
80. H. F. Ivey, Pt. I, *IRE Trans. Electron. Devices* **6**, 203 (1959); Pt. II, *J. Electrochem. Soc.* **108**, 590 (1961); Pt. III, *J. Electrochem. Tech.* **1**, 42 (1963). Pt. IV *Ibid.*, **3**, 137 (1965).
81. D. A. Cusano, *in* "Luminescence of Organic and Inorganic Materials" (H. P. Kallman and G. M. Spruch, eds.), p. 494. Wiley, New York, 1962.
82. P. Goldberg and J. W. Nickerson, *J. Appl. Phys.* **34**, 1601 (1963).
83. J. W. Nickerson and P. Goldberg, *in* "Tenth National Symposium on Vacuum Technology Transactions, 1963" (G. H. Bancroft, ed.). Pergamon Press, New York, 1963.
84. W. A. Thornton, *J. Appl. Phys.* **33**, 3045 (1962).
85. P. A. Jackson, Hull Conference on Luminescence, 1964, to be published.
86. M. Shiojiri and E. Suito, *Japan. J. Appl. Phys.* **3**, 314 (1964).
87. H. Berger, *Physica Status Solidi* **1**, 739 (1961).

The Mechanical Properties of Thin Condensed Films

R. W. HOFFMAN

Department of Physics, Case Institute of Technology, Cleveland, Ohio

I. Introduction

The mechanical properties of thin films have been studied from several points of view. The large internal stresses, first found in electroplated films, have been an annoying feature often leading to film fracture and peeling, although there exist a few examples where the planar stress has been useful in producing a desired pseudosingle crystal symmetry for certain film properties. Early observations of films exhibiting an unexpectedly high structural strength provided another motivation for the study of the mechanical properties of films. More recently, the correlation of structure and mechanical properties is leading to a better understanding of condensed films, but a quantitative theory of film mechanics seems to evolve only slowly.

Although the literature concerning the mechanical properties of films is not so extensive as in the case of the electrical and magnetic properties, we still cannot review every paper in detail. We shall set as our goal, then, to give a summary of the major research trends, together with a discussion of the physical models proposed to explain the experimental results. For the most part we shall be concerned with films of metals formed by evaporation techniques under various deposition conditions. Nonmetals will be considered when the corresponding information for metallic films is lacking, or where the different properties of such substances can give an insight into the particular physical mechanism studied. Films formed by sputtering and by

211

electroplating will not be discussed in detail, since the information is generally lacking for the former and too dependent on bath complications for the latter. As the correlation between structural details and mechanical properties unfolds, it will become increasingly clear that these properties do not depend on the particular mode of film formation, but only on the resultant structural order and impurity content.

II. Structural Considerations

The association of physical properties with structural details has been the objective of much of recent solid-state science. In the case of films, the high-resolution electron microscope has been perhaps the most important tool. Results have been discussed in a number of detailed reviews: "Structure and Properties of Thin Films," (Wiley, 1959), "Thin Films" (American Society for Metals, 1964), and the multivolume "Physics of Thin Films" (Academic Press, 1963ff.) deal with the present knowledge of the condensation process, and with crystal growth, textures, and epitaxy. In scanning the literature, it becomes apparent that most of the detailed structural information comes from epitaxial films condensed on substrates at elevated temperatures, whereas most of the mechanical data has been obtained from polycrystalline films condensed on ambient-temperature glass-like substrates. A critical review of the present status of film-structure research thus seems in order, if the proper correlations to the mechanical properties of films are to be achieved.

1. NUCLEATION AND GROWTH

Thun (1), Neugebauer (2), and Walton (3) have recently discussed the nucleation and growth of very thin layers, and several authors (4, 5, 6) have examined in particular the growth of Au, Ag, and Pb films under electron-microscope observation. They found the now well-known "liquid-like" behavior, in which the density of crystallization nuclei decreases, during deposition, by the coalescence of such nuclei. The nuclei are usually rounded, but exhibit sudden changes in shape when two join together in the early stages of growth. The mass-transport mechanism is believed to be surface diffusion. Reorientation of two crystallites has also been noted at this stage (7). As the growth continues, the nuclei become larger and grow together to form a network with many open areas.

These holes ultimately fill in and may be the source of the large dislocation density found in most epitaxed films (8). Twins, stacking faults, and other defects have been noted in large numbers for thicker (continuous) single-crystal films. These films have all been deposited on substrates held at elevated temperatures to reduce film contamination and to achieve epitaxy. Under

these conditions and with the materials so far studied, a high mobility is expected.

It is not clear whether the same pattern governs the nucleation and growth of polycrystalline films at lower temperatures on glassy substrates, but some information is available. Pashley et al. (6) indicate that a similar liquid-like coalescence occurs in polycrystalline films, and that large orientation changes and recrystallization take place as the growth proceeds. The resulting grain size of the deposit is large compared with the initial separation of the nuclei, since as many as 100 initial nuclei may contribute to each grain. The grain size is thus determined primarily by the recrystallization process rather than the density of initial nuclei. The details of recrystallization have not been worked out, but since a dependence of the crystallite size upon deposition rate has been noted, the final deposit may reflect to a degree the initial nucleation.

a. Preferred Nucleation. A characteristic of the mechanisms just discussed is the appearance of initial nuclei at an average thickness of a few angstroms. These nuclei may lie along the cleavage steps of a single-crystal substrate, they may be located at the intersections of dislocations with the surface, or they can form at point defects, or impurities (4). Prenucleation of the substrate with another extremely thin evaporated layer changes the growth considerably in the case of Zn, Sn, and Pb. Jeppesen and Caswell (9), for instance, prenucleated a NaCl substrate maintained at room temperature with 10 A of Cu, Ag, or Au, and examined the resulting 300-A Pb film by transmission microscopy and X-ray diffraction. The unnucleated lead film consisted of isolated grains with rounded edges. The Cu and Ag nucleation yielded similar open patches between grains, except that almost all the grains were connected by bridges. The Au nucleation, in contrast, produced an almost continuous film with much smaller crystallites. It was felt that the formation of a Au-Pb intermetallic compound was important in the nucleating process.

Similar fine-grained iron films on formvar substrates have been observed without prenucleation (10). In this case no well-defined isolated nuclei were found for films of 10 to 20 A average thickness, but rather a "fuzzy" two-dimensional maze-like structure. These maze formations were 50 to 100 A wide and appeared to consist of iron crystallites 10 to 20 A in size. An iron diffraction pattern was obtained, albeit broadened by strain and particle size. Conditions of low mobility resulting in continuous films of small crystallite size are probably more common than is generally realized.

The recent Mössbauer measurements on layered films of iron and SiO have shown that the internal field is the same as bulk for films down to 5 A, indicating a continuous film in this thickness range. In addition, Lee et al. (10a) found a two-line spectrum for thinner films, demonstrating a narrow

distribution of crystallite sizes. 25-A-thick films were examined by electron microscopy and found to be continuous.

b. Angle-of-Incidence Effects. Smith *et al.* (*11*) have found that chains of crystallites oriented perpendicular to the plane of incidence are developed when the incident vapor beam forms a large angle with the substrate normal. Direct confirmation by electron microscopy was available for thinner films, and optical dichroism as well as magnetic measurements suggested that these chains are also present at greater film thickness. Resistivity anisotropies also resulted, according to Pugh *et al.* (*12*) and Smith *et al.* (*13*), from large angles of incidence. The mechanism for this chain formation is a geometric "self-shadowing" in which the initial random nuclei shield the substrate from the vapor beam. As the film grows, vacant areas remain on the substrate, but the crystals ultimately grow together to form long chains. It is felt that this condition would hold only for films evaporated under conditions of low mobility, but this is disputed by Behrndt (*86a*). Although these effects would clearly be important for very thin films, their role may be less pronounced for a continuous film unless anisotropic growth is obtained. Both maze and chain-like structures were found in electron micrographs of iron deposited at 36 degrees incidence (*10*). Chains both parallel and perpendicular to the plane of incidence were found at depositions between 100 and 150°C, but only a random maze at lower substrate temperatures.

2. STRUCTURE

A correlation of mechanical properties and structure requires knowledge of the distributions of crystallite size and orientation, as well as the density of planar, linear, and point defects in the films as deposited and after subsequent annealing. It is thus appropriate to discuss some of these structural features as they are found in polycrystalline and single-crystal films.

a. Polycrystalline Films. The crystallite size increases as the substrate temperature is raised. Fleet (*14*) has carried out a detailed study of nickel films condensed on glass or fused silica at condensation rates of 3 to 12 A/sec. For room-temperature substrates the crystallites had diameters of about 60 A, and the films were several crystallites thick. At substrate temperatures of about 350°C, large flat crystals measuring about 1000 A across and extending through the film were surrounded by regions several crystallites thick and 500 A in diameter. At still higher temperatures the film became one crystallite thick throughout and the crystallites measured several thousand angstroms across. Figure 1 indicates the average crystallite size as a function of substrate temperature for 500-A-thick nickel films, showing the onset of the large crystallites at about 350°C.

The condensation rate also effects the crystal size. Thun (*1*) gives some data for 1000-A chromium films at various substrate temperatures. For 25°C sub-
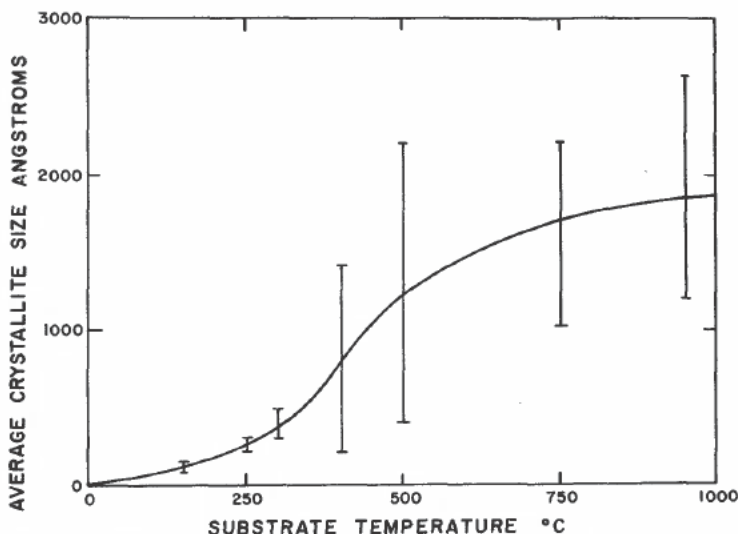
FIG. 1. Crystallite size in 500-A nickel films as a function of substrate temperature. [Data from Fleet (14).]

strate temperature the grain diameter was independent of the rate between the limits of 10 and 500 A/sec, whereas higher substrate temperatures resulted in a constant grain size only up to a threshold rate at which the grain size began to decrease rapidly with increasing rate. This behavior indicates that the crystal size became limited by a process in which the high-mobility surface atoms were buried before they could reach an ordered lattice site. Campbell *et al.* (15) also observed, for gold and lithium fluoride, smaller crystals at larger evaporation rates, similar to earlier measurements by Sennett and Scott (16), who found more agglomeration in silver at low evaporation rates.

For a fixed condensation rate and substrate temperature the crystallite size depends on the average film thickness. Figure 2 presents Fleet's results for nickel at a substrate temperature of 150°C. Up to a thickness of 250 A grain size increases almost linearly, and then decreases slowly to a constant mean diameter of about 100 A. This implies that either new crystals are nucleated as the film continues to grow, or that existing crystals are broken up. Lithium fluoride behaves similarly. Its crystallite size increases up to a film thickness of about 100 A, and then decreases slowly to an average area of $2 \times 10^4 \, A^2$ for thicknesses greater than 200 A. As a result of these observations, Campbell *et al.* (15) developed a specific model for the nucleation and growth of LiF.

Gold shows also an initially increasing crystallite size, at least up to an average film thickness of 100 A.

It is not clear whether the crystallites extend through the thickness of the film. Columnar growth is well known in electroplated films at particular current densities and temperatures, and with certain additions to the bath. Nickel films are, according to Fleet (14), several crystallites thick when deposited at lower substrate temperature, but consist of only a single layer of thick crystallites when condensed at a high temperature. Blakely (17) indicates, on the other hand, that polycrystalline gold films deposited at only 40°C consist
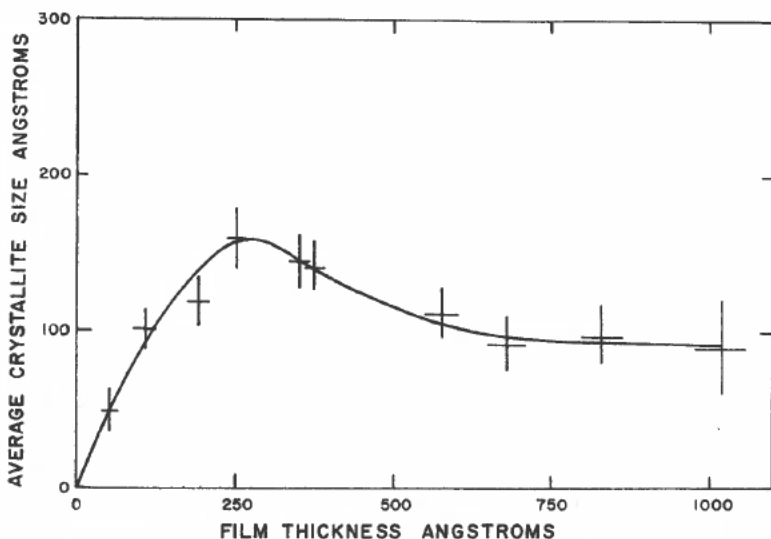
FIG. 2. Crystallite size in nickel films evaporated at approximately 10 A/sec on substrate at 150°C as a function of film thickness. [Data from Fleet (14).]

usually of grains which extend from one surface to the other. He found a mean grain diameter of about 200 A, much less than the 800-A thickness of the gold films.

During the growth of polycrystalline films on carbon substrates at about 400°C, Pashley (6, 8) has observed large reorientation effects when the nuclei coalesce. The orientation difference between adjacent crystallites, however, covers a range including large angles. Some information on this point is available from the work of Palatnick et al. (18) using electron-diffraction microbeam techniques on aluminum films of 60 to 200 A thickness which had been condensed on cool substrates. They found that the small crystallites or "block

crystallites" extended through the thickness of the film. Reduction of the aperture and hence the diffracting volume reduced the number of spots in a given ring and increased the average angle between spots, indicating that most blocks have a large orientation difference with their neighbors. If the blocks were assumed to be cubes, the average length would be greater than the film thickness, but even so, the block crystallite size was felt to be determined by the thickness of the film.

The crystallite size may undergo large changes upon annealing. Palatnik *et al.* indicate that the random diffraction ring tends to disappear, leaving only isolated spots as a proof of the microrecrystallization which takes place. Upon further heating, the number of spots decreases, indicating that the larger crystallites grew at the expense of those which are smaller and more randomly distributed. Grain growth in iron during heating has been qualitatively observed by Vesely and Hoffman (*10*) in the electron microscope. Their study confirms the fact that the extremely small crystals (<100 A) in a condensed film undergo rapid changes and increase in size by a factor of 5 to 10. The recrystallization seems to stop rather suddenly at a crystallite size many times larger than the thickness of the film. This final structure contains voids between some crystallites. Recrystallized grain diameters of about 1000 A can be found in films of an average thickness of about 50 A. It is not yet known whether this growth pattern is similar to the recrystallization by coalescence observed in cold-rolled foils by Hu (*19*). Blakely has observed the microstructure changes in annealing carbon-coated gold films on a 600°C hot stage in the electron microscope. His observations indicate that aggregation occurs in two stages: first, recrystallization to a stable grain structure, and then separation of individual grains along the stationary grain boundaries. It is suggested that a diffusion process is responsible for this behavior.

Gimpl *et al.* (*19a*) have recently annealed continuous nickel and gold films to high temperatures and studied the resulting recrystallization and island formation. They observed amorphous NiO as well as an unidentified amorphous gold film occupying the area between the islands, in contrast to previous workers who have interpreted such structureless areas on micrographs as cracks in the films.

Bachmann *et al.* (*19b*) finally have studied the morphological changes in copper films during annealing and oxidation, and in particular examined very thin (10 to 50 A) deposits on both carbon and SiO substrates. For carbon substrates they found at 500°C a large increase in crystallite size approaching 1000 A in diameter, whereas little or no change was noted for the films on SiO substrates. Thicker (100 to 200 A) deposits, although still not continuous showed a growth on SiO substrates only if the original deposit consisted of large, interconnected islands. The authors suggest that for the thicker continuous films the mass transport occurs by self-diffusion of copper, whereas

for island films the copper must migrate over the substrate surface. This surface diffusion is indeed slower for SiO than for carbon substrates.

The internal structure of individual crystals in a polycrystalline film is similar to those observed in epitaxial films, but has not yet found detailed interpretation. It is probably safe to assume that dislocation densities will be at least as high as those found in epitaxial films, and other imperfections are undoubtedly present as well. We shall not consider allotropic transitions except to remark that such changes will be reflected in the mechanical as well as other properties.

b. Films with Preferred Orientation. Fiber textures have been noted in films for a long time [see, for instance Evans and Wilman (20)]. Mixed textures are common, as well as a partial texturing together with some random crystallites. The texture axis is perpendicular to the film for atoms arriving perpendicular to the substrate, and is usually inclined toward the vapor stream for other angles of incidence. Since none of the models for the mechanical properties are sufficiently detailed to take account of any local orientation differences, we face the same interpretation problems as for the random-oriented poly-crystalline films. A film with a strong fiber texture would normally have different elastic constants for the texture axis and the axis normal to it, but these differences cannot account for the anisotropic stresses actually observed. For the case of an inclined fiber axis, the elastic constants would be an intricate function of the angle between the direction of measurement and the texture axis. These anisotropies would probably not be large, since most fiber textures are not well developed. It is also not clear that an anisotropy in the elastic constants of the film would be reflected in a measurement of the internal stress, because it is really the strain in the substrate which is measured, and from which the stress in the film is inferred. Hence at the moment we need not treat textured films as being particularly different from random-oriented films.

c. Single-Crystal Films. As compared to other structures, we probably know most about the growth and structure of single crystals and least about their mechanical properties. The growth conditions for single-crystal films are now reasonably well known, and in any event do not concern us here. A reorientation of the joining nuclei is common during film growth [see Bassett (7) for the case of silver on molybdenite]. Once a continuous film is formed, a second twinned layer may develop, according to Jacobs and Pashley (21). (The boundaries between the two twin-related orientations possible in silver or gold on mica are at first perpendicular to the plane of the film; but after the film becomes continuous, parallel boundaries develop.) In silicon stacking faults develop at the boundaries of the joining grains (22). It is found that the dislocation density in epitaxial films is large, perhaps 10^{10} to $10^{11}/cm^2$; many twins and stacking faults are found also (6). Dot-like

features tentatively identified as vacancy aggregates or small dislocation loops were later seen to arise during the exposure to the electron beam, probably as a result of surface contamination (23). Annealing of single-crystal films does not seem to reduce the dislocation concentration appreciably, a behavior which is in contrast to that of bulk material, although annealing experiments with films free of the constraint of a substrate may add new information.

3. SURFACE STRUCTURE

As discussed in some detail by Thun (1), the density of a film may be considerably smaller than that of the bulk material. X-ray diffraction diagrams indicate, however, that the density within the crystallites is near normal. This implies that the low over-all density of films arises from voids between islands when the films are discontinuous or from high concentrations of oxide or other impurities, as well as vacancies at the grain boundaries for continuous films. Surface-area measurements [see Beeck et al. (24), for example] also indicate that the surface is anything but smooth on an atomic scale. Allen et al. (25) found that copper films deposited at low temperatures have a surface area linear with mass. This implies a film consisting of loosely packed particles. At higher substrate temperatures this linear relation is no longer observed.

Even in high vacuum a surface oxide or nitride layer will form in rather short times. Since all tensile measurements and some of the stress measurements have been made outside a vacuum system, we expect that these measurements include contributions from such chemical changes, and thus may not represent data characteristic for pure films. As these surface layers are generally quite thin, any contribution is expected to be small for thick films.

III. Internal Stresses

Since the work of Stoney on electroplated films in 1909 (26), the existence of large internal stresses has been known. Evaporated films were studied in the 1950's with the aim of understanding the origin of these stresses. In the following sections we shall review the measurement techniques, summarize the experimental results, and present models for their origin.

1. EXPERIMENTAL TECHNIQUES

a. Bending-Plate Methods. The stress has commonly been determined by observing the deflection of the composite of film and substrate during or after film deposition. For most of the experiments a long thin beam was used, either clamped at one side for an observation of the deflection of the free end, or held on knife edges for measuring the center deflection. In the case

of the cantilever beam, the deflection has been observed optically (27–29), through a capacitance change (30), or mechanically by using a surface-analyzer probe (31). An electromechanical (32, 32a) or magnetic restoration (33) of the null position in combination with a measurement of the restoration force has also been used. Some of these methods are sufficiently sensitive to permit stress measurements during the stage of initial film growth.

Table I compares the sensitivities of various techniques for measuring the

TABLE I

SENSITIVITY OF STRESS-MEASURING TECHNIQUES

Method of observing deflection	Type of plate[a]	Detectable force per unit width, dyne/cm	Ref.
Optical	B	800	63
Capacitance	C	500	30
Optical	C	250	27
Magnetic restoration	C	250	33
Electromechanical restoration	C	150	32
Mechanical	C	1	31
Electromechanical	C	1	32a
Interferometric	C	0.5	
Interferometric	P	15	41
Ferromagnetic resonance		1000[b]	49
X-ray		500[b]	35

[a] B, beam supported on both ends; C, cantilever beam; and P, circular plate.

[b] Approximate equivalent; a force is not measured.

deflection following Blackburn and Campbell (31) and Klokholm (32a). The sensitivity values quoted are a measure of the smallest detectable force per unit width using the conventional substrate geometry for the particular method. For thicker films any method will suffice, although those amenable to auto-matic recording might be preferred. For studies of the initial stages of growth, a sensitivity of at least the interferometric method is needed. The sensitivities may be increased by a factor of about five by choosing thinner substrates, but limitations in the validity of the usual plate equations represent a serious constraint. The methodical details of each approach can best be found by consulting the original papers.

The deflection of a circular plate has also been used for stress measurements (34, 35). The change in the optical fringe system between the plate and an optical flat is here used to measure the deflection of the plate. Because of the limited flatness of available substrates, the substrate profile is remeasured after the film has been dissolved and then used as a reference profile. (Fused

quartz substrates are generally flatter than glass, but, on the other hand, have more severe thickness gradients.) The fringe technique is illustrated in Fig. 3, and the photograph of an actual fringe pattern is shown in Fig. 4. It can be seen that the circular plate offers the possibility of observing stress anisotropies. Anisotropy has also been observed by Priest *et al.* (*36*) by using two orthogonal cantilever beams.
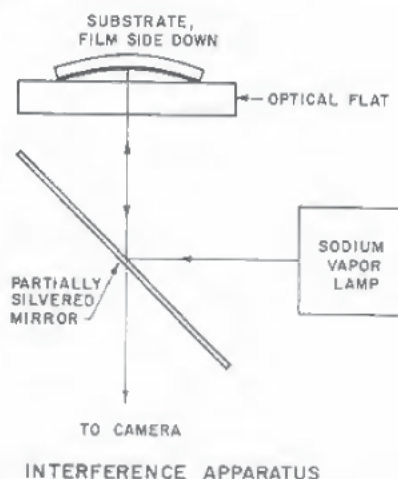
FIG. 3. Schematic drawing of circular fringe apparatus. Lenses may be needed if apparatus is used in vacuo. [After Finegan and Hoffman (*41*).]

FIG. 4. Observed fringe patterns. The circular fringes are observed for film evaporated at 0′ angle of incidence and the elliptical rings correspond to a beam incident from the top inclined 22.5 to the substrate normal. [After Finegan and Hoffman (*41*).]

In both the beam and the plate methods, it is elastic theory which yields the film stress as a function of the measured deflection. It is assumed that the film strains the substrate, which bends until equilibrium is reached, and that the film-substrate bond is strong enough to suppress slippage, a condition that seems to be fulfilled in practice. Since the film stress is computed from the observed substrate strain only, it is apparent that the elastic constants of the film are not taken into consideration in this approximation.

The equation derived by Stoney is

$$\sigma = \frac{Ed^2}{6rt} \tag{1}$$

where σ is the stress in the film, E Young's modulus for the substrate, d the substrate thickness, t the thickness of the film, and r the radius of curvature of the bent strip. This equation can easily be transformed to an expression relating the stress to the deflection of a cantilever or otherwise supported beam. The stress is defined as tension if the plate bends in a way decreasing the film length, and compression if the film tends to expand. Brenner and Senderoff (37) pointed out that Eq. (1) neglects some important features. First, it ignores the stress change in the film as the substrate curvature changes during condensation. This change induces a stress relief, which in turn depends on the total amount of deflection. A second error arises from the fact that the beam is really a composite structure of film and substrate, and that this results in a different equation if the elastic moduli of film and substrate differ. A correction can be obtained by replacing the composite beam with an equivalent T beam, where the widths of substrate and film are proportional to their moduli. The neutral axis and stiffness can now be calculated by standard beam theory. Brenner and Senderoff have further distinguished between three experimental cases during the deposition of the film: rigid constraint so that neither contraction nor bending can take place, constraint from bending but not from contraction, and no external constraints. They also considered the effect of temperature changes. Their equations apply to cases where the film thickness is an appreciable fraction of the total beam thickness and the resultant corrections to Eq. (1) are less than about $5t/d$. For a typical film thickness of about 2000 A and a substrate thickness of 0.005 cm, however, all these corrections to Eq. (1) amount to only about 0.4% and are thus negligible.

Equation (1) implies still another serious simplification. The elastic theory of simple beams was used in its derivation, but the bending of substrates by films should really be treated as the bending of a thick plate (38). The theory of plates yields for an isotropic stress in equilibrium with the resultant strain,

$$\sigma = \frac{Ed^2}{6(1-v)rt} \tag{2}$$

where v is Poisson's ratio for the substrate and the other symbols have their previous meaning. Note that the stress is increased by the factor $1/(1 - v) = \sim 1.5$ if plate theory is used. The reader is warned that most of the stress values in the literature have been calculated from Eq. (1) rather than the proper equation (2). As in the previous case, Eq. (2) may be modified for a particular type of substrate support. Young's modulus can be obtained by measuring the plate deflection under a given load.

The theory presented so far is limited in its application to bending displacements, which are small compared to the thickness of the plate. Since actually measured displacements are often not much smaller than the substrate thickness, it must be asked whether or not the simple theory can be applied. No general answer can be given, but Timoschenko has solved the problem for large plate deflections if a bending moment is applied only to two opposite edges of the plate (39), a condition which is very similar to the film-substrate case. The substitution of displacement data for films in Timoschenko's equation yields results which are essentially the same as those obtained with the simple plate theory, indicating that the latter is reasonably accurate. Whenever deflections comparable to the plate thickness are encountered, it might nevertheless be prudent to examine if this assumption is also valid for the experimental conditions chosen.

Equation (2) neglects the stress relief as well as the small change in stiffness as the film is built up. A numerically integrable solution including these corrections, as well as the Poisson term and different elastic moduli for film and substrate, has been given by Davidenkov (40). However, as we saw in the case of the simple beam theory, these effects are small as long as the film thickness is much less than the substrate thickness.

Often the beam stiffness is measured by applying a known force and observing the resulting deflection. This measurement also involves the bending of a plate rather than a beam. For an end-loaded cantilever plate, the proper equation for the average force per unit width is (32a)

$$T = KF(1 + v) \tag{3}$$

where K is a constant involving the dimensions of the plate and F is the loading force applied to the end of the beam which produces the same deflection as the film. In all these cases it is assumed that the plate is long compared to its width.

If the stresses are anisotropic, the shape into which an isotropic and flat substrate of constant thickness will be deformed has been calculated by Finegan and Hoffman (41), with the result

$$z = \frac{3(F_x - vF_y)x^2}{Ed^2} + \frac{3(F_y - vF_x)y^2}{Ed^2} \tag{4}$$

where z is the displacement of the plate perpendicular to the substrate plane at a particular point (x, y), and F_x and F_y are the forces per unit width in the x and y directions. Equation (4) is valid as long as the displacement z is no larger than one-tenth of the substrate thickness. A measurement of the shape of the deformed substrate in orthogonal directions will yield values for the tensions per unit width. The tensions per unit width are related to the average film stresses by the equations

$$F_x = \sigma_x t; \qquad F_y = \sigma_y t \qquad (5)$$

where σ_x and σ_y are the stresses in the x and y directions. A graphical technique for the reduction of the data obtained from an optical fringe pattern is given in the paper by Finegan and Hoffman; a computer solution was also developed.

The general solution for an anisotropic substrate has not been evaluated, although it would be of interest for the growth of epitaxial films. The solution is known, however, for a thin single-crystal substrate of cubic structure which is elastically isotropic. The moduli for a substrate orienting the $\langle 111 \rangle$ direction perpendicular to the film plane are (42)

$$E^{-1} = s_{11} - \tfrac{1}{4}[2(s_{11} - s_{12}) - s_{44}]$$

$$v = \frac{-s_{12} + \tfrac{1}{12}[2(s_{11} - s_{12}) - s_{44}]}{E^{-1}} \qquad (6)$$

where the quantities designated s are the usual elastic compliances.[1]

All stress determinations discussed so far assume that the stress is uniform throughout the film thickness. The observation that peeling films usually curl away from the substrate, however, by itself suggests that the stress in films is really not uniform. In studies of electroplated films the term "instantaneous" stress has frequently been used, designating the stress in an infinitesimally thin surface layer of the growing film. The instantaneous stress is proportional to the slope of the deflection-thickness curve and can thus easily be obtained from a continuous observation of the substrate deflection. The slope of the tension per unit width-thickness curve becomes identical to the instantaneous stress, if the contribution due to the composite beam is in both cases ignored. The thickness dependence of the stress is clearly documented by showing the change in instantaneous stress (43). The average stress, however, is quoted more frequently.

[1] The first published report of the use of single-crystal substrates seems to be Glang et al. (42a). They have measured the stress in molybdenum films on $\langle 111 \rangle$ silicon wafers. Dumin (42b) has measured the stress in epitaxial silicon films vapor-grown on sapphire at 1100°C. The thermally induced stress in the silicon was about 5×10^9 dynes/cm^2 compression.

Since film and substrate form a sandwich consisting of two materials with different coefficients of thermal expansion, temperature effects also enter the picture. Stresses arise whenever the deposition temperature differs from the temperature at which a measurement is made. The thermal-expansion co-efficient of a film may actually be determined by a stress measurement, provided the substrate temperature is known accurately. It is unfortunately difficult to clamp the substrate sufficiently tight to a heat sink to permit a precise temperature measurement, and to provide also for the free movement required for a stress determination. As yet no good solution to this problem has been found, although using a liquid-gallium contact to a copper heat sink was at least partially successful (44). The temperature rise during deposition has been estimated by Pashley et al. (6) for the case of slow evaporation rates on extremely thin substrates. The temperature rise amounts under these con-ditions to only 0.25°C. The temperature rise at more normal deposition rates is larger but does probably not exceed 50°C for a conventional evaporation geometry. This presents a minor uncertainty in separating the thermal and intrinsic contributions to the stress in thin films.

Thermal gradients through the thickness of the substrates also induce a bending of the film-substrate combination which may falsely be interpreted as a film stress. This stress contribution is most bothersome when the deflec-tion is monitored continuously, and often it appears as a compression rather than the usual tension. An analysis of this effect has been given by Blackburn and Campbell (31) for the case of LiF films deposited at 50 A/sec. The total temperature rise after an extended evaporation was calculated to about 50°C, and the temperature difference across the glass substrate to 0.03°C. Experimental verification was obtained for short time intervals under the assumption of a constant temperature gradient. Klokholm has found a large difference between a dynamic (continuous) run and a sequential evapo-ration in which the substrate was permitted to reach thermal equilibrium before the measurement was taken.

b. *X-Ray and Electron-Diffraction Methods.* Stresses may also be deduced from the measurement of a change in lattice parameters. X-ray techniques are preferable to electron diffraction because of their higher resolution, owing to the larger Bragg angles. Kinbara (45) and Kinbara and Haraki (46) have measured the lattice constant perpendicular to the film plane by diffracto-meter techniques. The strain is measured directly, and the isotropic stress is then computed from

$$\sigma = \frac{E}{2v_f} \frac{a_0 - a}{a_0} \tag{7}$$

where a_0 and a are the lattice constants of the bulk material and the (strained)

film, respectively. A smaller lattice constant perpendicular to the film corresponds to a tensile stress; negative values of σ indicate compression.

The stress in the film can also be obtained from a measurement of the lattice constant in the film plane, although the geometry is here more suitable for electron diffraction. The stress is given in this case by

$$\sigma = \frac{E}{1 - v_f} \frac{a - a_0}{a_0} \tag{8}$$

Halliday *et al.* (*47*) have published a detailed treatment of stress determinations by electron diffraction.

Freedman (*48*) has measured X-ray strains in single-crystal nickel films, in which case the stresses must be calculated for the cubic symmetry:

$$\begin{aligned}
\varepsilon_x &= s_{11}\sigma_x + s_{12}\sigma_y \\
\varepsilon_y &= s_{12}\sigma_x + s_{11}\sigma_y \\
\varepsilon_z &= s_{12}\sigma_x + s_{12}\sigma_y
\end{aligned} \tag{9}$$

where the ε's are the strains and the σ's the stresses in the x, y, and z directions.

It should be pointed out that the surface of the film is without constraint, hence $\sigma_z = 0$, and that ε_z is therefore the Poisson contraction normal to σ_x and σ_y. The thermal strain normal to the film and the strain energy for several simple orientations in the cubic system have been calculated by Vook and Witt (*48a*). They assumed that the shear strains normal and in the plane of the film were zero, in addition to the assumptions stated above.

c. Other Techniques. The existence of a stress will produce an anisotropy in ferromagnetic films as a result of the magnetoelastic coupling. Since the resonant frequency depends on the anisotropy as well as the magnetization, a shift in the resonance peak will occur. With proper geometry this can be separated from other anisotropy shifts, and the stress can be calculated. MacDonald (*49*) was the first to use this technique to measure stresses, but its somewhat limited applicability does not warrant a more detailed description.

2. Summary of Experimental Results for Various Metals and Nonmetals

The stress in a thin film, as measured by one of the methods discussed in the previous section, consists of two major components. One results from the different thermal-expansion coefficients of film and substrate combined with the difference between the deposition temperature and the temperature prevailing during the measurement; the other, sometimes referred to as the

"intrinsic" stress, arises from film contamination and the incomplete structural-ordering processes occurring during film growth. We shall first treat the thermal stresses and then discuss the dependence of the intrinsic stress upon deposition parameters and materials.

a. Thermal Stress. This stress component can be calculated with good accuracy from the difference of the bulk expansion coefficients, and it does not exhibit any unusual behavior. Some experimental difficulties are usually encountered, however, in measuring accurately the film temperature during deposition, as every experimenter knows. This contribution of the differential expansion to the total stress can vary widely, depending on the substrate temperatures during deposition and measurement and, of course, the film and substrate materials.

The computation of the differential-expansion stress is straightforward if the substrate is thick enough that its bending during the temperature changes can be neglected. The constraints imposed by the bonding then give the following strain value if the temperature is constant during evaporation:

$$\varepsilon_T = (\alpha_f - \alpha_s)\,\Delta T \tag{10}$$

where α_f and α_s are the average coefficients of expansion for film and substrate and ΔT is the temperature of the substrate during evaporation minus its temperature at measurement. The stresses are obtained by multiplying the strain value with the appropriate modulus. The sign agrees with the usual practice: It is positive for tension, negative for compression. The coefficient of expansion is about 8 for glass, 10 to 20 for many metals, and 30 to 40 for the alkali halides, all in units of $10^{-6}/°C$. Since ΔT as defined in Eq. (10) is usually positive, a tension stress is found for metals on glass, but a compression stress for metals on alkali-halide substrates. For nickel films deposited at 75°C on soft glass and measured at 25°C, the differential expansion contributes about 5% to the total stress. As the substrate temperature is raised, the differential-expansion term increases and the intrinsic stress decreases, until the differential thermal expansion becomes at about 250°C the only contributor. In practical film applications, the stresses produced by differential expansion are often large and can be of either sign, but they are at least amenable to calculation, and they can frequently be controlled by a judicious choice of substrate material and deposition temperature.

It follows that stress-sensitive properties differ for deposited films and bulk samples, and such differences actually have been observed for electrical, magnetic, and superconducting properties. In a study of the effect of elastic strain on the superconducting transition of tin films, for instance, Blumberg and Seraphim (*50*) found that the critical temperature increased with decreasing film thickness. This agrees with a model in which the stresses arise from

thermal expansion and reach a maximum which is determined by the critical shear stress arising from dislocation pinning at the film surfaces.

Thermal strains in semiconducting films epitaxially grown on NaCl are sufficiently large that the energy band gap is slightly changed [see Zemel (*50a*) for example]. In principle, the stresses could be measured by this technique.

Freedman (*48*) has discussed the thermal expansion of epitaxially grown films. He found for a nickel film on an NaCl substrate that the elastic distortions were at 275°C sufficient to induce a tetragonal film structure. On the other hand, when the film was stripped from the substrate, it showed its normal lattice parameters. The stress was compressive and amounted to -1.0×10^{10} dyne/cm².

b. Intrinsic Stress. This second contribution to the total stress is more interesting since it reflects the growth of the film in a way not well understood at present. Even the experimental data published by different authors on the intrinsic stress are not very consistent. Since the stress does mirror somehow the film structure, we expect a thickness, condensation rate, and deposition-temperature dependence. Some of the scatter of experimental data undoubtedly arises from variations in these parameters.

The average stress in thick films is relatively independent of the film thickness. Table II gives average stress values for various metal films approximately 1000-A thick, listing other deposition data as well. Note that the stress does not seem to depend strongly on the substrate material, even though such a dependence is expected. According to the usual practice the values have not been corrected for the Poisson term in the bending. The total stress is given in some cases for lack of more detailed information. All values should be considered representative rather than precise.

Since the force per unit width is a convenient stress measure for films, some force-per-unit-width data resulting from continuous growth observations are presented in Fig. 5 for several metals. The permalloy data are based on work by Weiss and Smith (*51*), and the nickel data on a study by Klokholm (*52*). Both sets of data have been obtained with a cantilever beam, and neither is corrected for the Poisson term. The iron data have been measured by Riesenfeld and Hoffman (*53*) on a circular plate, and they include the Poisson correction. Earlier data measured on individual iron (*41*) films indicated an unexplained peak near 700 A which was very likely caused by some mechanical instability in the substrate. The rates of evaporation for the permalloy and nickel films were considerably lower than the 60 A/sec used in the iron depositions. The nickel was condensed at room temperature, the iron at 75°C, and the permalloy at 225°C. Average stress values may be obtained by dividing the force-per-unit-width data by the film thickness. They fall into the expected range of $\sim 10^{10}$ dyne/cm². The average stress for permalloy and nickel is almost constant. Iron exhibits a constant force term

TABLE II

INTRINSIC STRESSES IN METAL FILMS APPROXIMATELY 1000-A THICK

Metal	Substrate temp. °C[a]	Substrate material	Stress, 10^9 dyne/cm^2	Sign[b]	Method[c]	Ref.
Ag	90	Glass	0.75	T	C	30
	A	Copper	1.0	T	T	54
	A	Mica	0.2	T	C	56
	A	Copper	0.75	T	C	27
Al	A	Cellulose	1.2	T	ED	78
	A	Copper	0.1	T	C	27
Au	A	Cellulose	4.6	T	ED	78
	A	Quartz	2.9	T	P	45
	A	Copper	0.85	T	C	27
Cu	A	Copper	0.9	T	C	27
	25	Mica	0.2	T	B	63
	A	Cellulose	4.4	C	ED	47
	A	Copper	1.5	T	C	55
	75	Mica	0.1	T	C	32
	−150	Mica	3.6	T	C	32
Ni	A	Glass	5–8	T	P	58
	A	Copper	3.5	T	C	27
	A	Glass	7.7	T	C	52
	75	Mica	6.4	T	B	63
	175	Mica	2.6	T	B	63
	A	Mica	5–8	T	FR	49
Fe	75	Mica	10.5[d]	T	B	38
	175	Mica	5.9[d]	T	B	38
	75 + A	Glass	9.6[d]	T	P	41
	A	Glass, silica	8.5[e]	T	P	53
	A	Copper	3.1	T	C	27
Permalloy	75	Glass	9	T	P	58
	75	Glass, mica	9	T	C	51
Sb	A	Copper	0.8	T	C	93
	A	Copper	0.25	T	C	27
Co	200	Glass	3.4	T	B	63
Pd	A	Copper	1.4	T	C	27
Mg	A	Copper	0		C	27
Bi	A	Copper	0		C	27
Zn	A	Copper	0		C	27
Pb	A	Nickel	0		C	65
Sn	A	Glass	0		C	50
In	A	Silica	0		C	64

[a] A means thermally floating at ambient temperature.

[b] T refers to tension, C to compression.

[c] B, beam supported on both ends; C, cantilever beam; ED, electron diffraction; and FR, ferromagnetic resonance.

[d] Poisson-corrected.

[e] Poisson-corrected, 36.5° angle of incidence.

superimposed on a force term which increases almost linearly with thickness for thicknesses greater than 400 A. The average stress thus decreases with increasing thickness.

Copper, silver, and gold have been measured by the University of Tokyo group. Their average stress data are shown in Fig. 6. The copper and silver
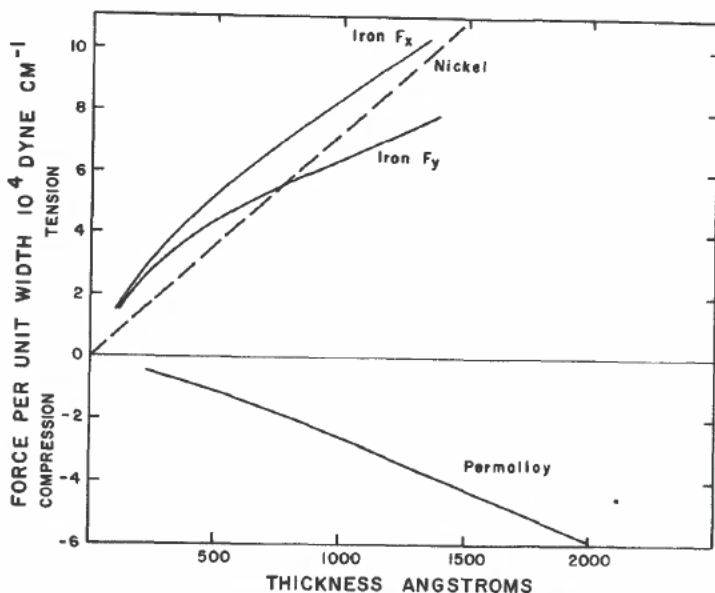
FIG. 5. Force per unit width for several metals as a function of film thickness. Data points are omitted for clarity; the curves represent average values. The iron data illustrates the stress anisotropy for a 36.5°-angle-of-incidence film and has been corrected for the Poisson term. [Data: Permalloy, Weiss and Smith (51); nickel, Klokholm (52); iron, Riesenfeld and Hoffman (53).]

data were obtained by both continuous and sequential observations, sensing the deflection of the copper cantilever by capacity changes. The silver data (K) have been published by Kato et al. (54), the copper values by Horikoshi et al. (55). Additional silver (KKS) data by Kinosita et al. (56) have also been included. All films exhibit no stress until they reach thicknesses of a few hundred angstroms, at which point a sudden stress rise to an almost constant level can be observed. These threshold thicknesses coincide roughly with the thickness at which the growing nuclei touch each other, according to observations on films evaporated under similar conditions. This behavior is emphasized if the stress distribution is plotted against thickness (Fig. 7). The thickness dependence of the stress is hyperbolic for the (KKS) silver films, and thus
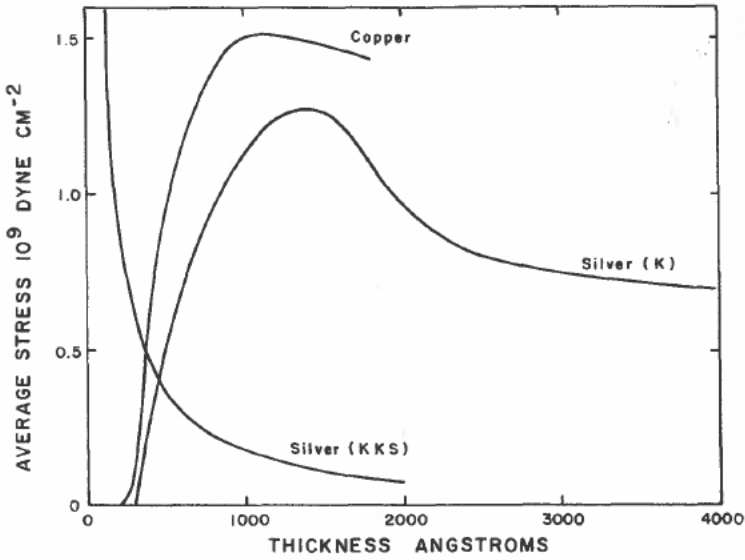
FIG. 6. Average stress as a function of thickness. [Data: copper, Horikoshi *et al.*; (*55*), silver (K), Kato *et al.* (*54*); and silver. (KKS), Kinosita *et al.* (*56*).]
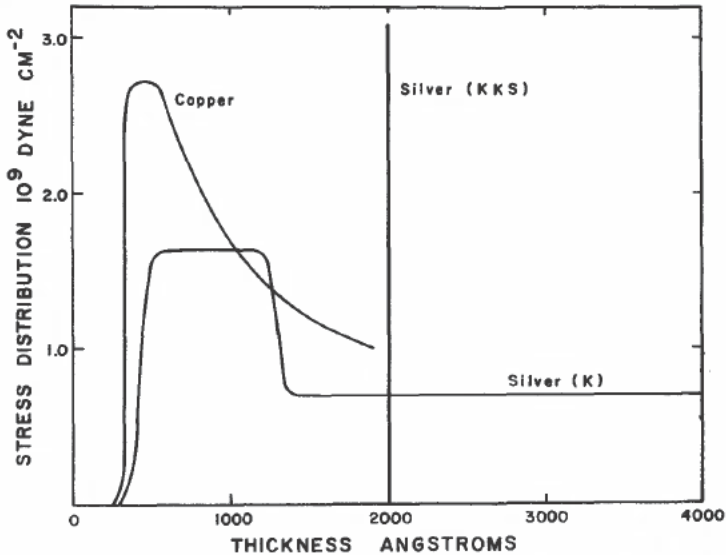
FIG. 7. Stress distributions in copper and silver. Data as marked in Fig. 6. The silver (KKS) is arbitrary to show all stress developed in the free surface layer.

fits a model in which the stress is constrained to a thin layer, and is effectively zero throughout the remainder of the film. According to Kinosita *et al.*, the stress should be concentrated in a 10-A layer near the free surface, since the films show a concave free surface when they are detached from the substrate. New data for silver by Kinosita *et al.* (*60b*) do not show this hyperbolic behavior.

The internal stresses in gold films condensed on room-temperature quartz substrates at 15 A/sec have been measured by Kinbara (*45*), using X-ray methods as well as the circular-plate technique. Both methods yield similar data at small thicknesses, but their results differ for thicker films, where the X-ray technique gives an almost constant stress (Fig. 8). An interpretation of these data indicates that the films are composed of a 1000-A-thick base layer of inhomogeneous stress and a superposed region of uniform stress.

A somewhat similar thickness-dependent stress behavior has been found by Horikoshi and Tamura (*43*) for antimony. Their measurements were also made by observing the deflection of a cantilever beam during evaporation. They found zero or very small stresses up to a thickness of several hundred angstroms, followed by a rapid stress increase in a narrow thickness range. For thicknesses greater than about 1000 A, the stress approached an approximately constant value (Fig. 9). The corresponding stress distribution (also shown in Fig. 9) indicates that almost the entire stress is confined to a narrow thickness region at about 1000-A film thickness. Since the authors found from electrical measurements that their films changed from amorphous to crystalline at this thickness, they concluded that the major contribution to the intrinsic tension is caused by the crystallization process. Compression was observed at faster (30 to 150 A/sec) rates and higher ($> 50°C$) temperatures, but this compression stress was largely caused by thermal gradients in the sample and in most cases vanished later. To avoid such thermal effects, the measurements must be made after the deposition is interrupted and the substrate cooled to a stable temperature.

Between -150 and $200°C$ susbstrate temperature metals commonly exhibit tension. The tension decreases with increasing substrate temperature, often linearly, and finally changes at a higher temperature to compression. Figure 10 shows typical data for the substrate-temperature dependence of the stress in copper, nickel, iron, and permalloy. The permalloy data (P) represent the total measured stress at room temperature; the others are intrinsic stresses. The point at which the tension goes to zero or to compression is reached for low-melting metals at relatively low temperatures. The copper data are from Horikoshi *et al.*, the permalloy data (P) from Prutton (*58*), the permalloy data (W) from Weiss and Smith, and the nickel and iron data from the Case group. The permalloy curves indicate some influence of the deposition rate on the average stress, and Horikoshi *et al.* reported for copper films a similar rate dependence. They found that the stress increased with increasing rate, but
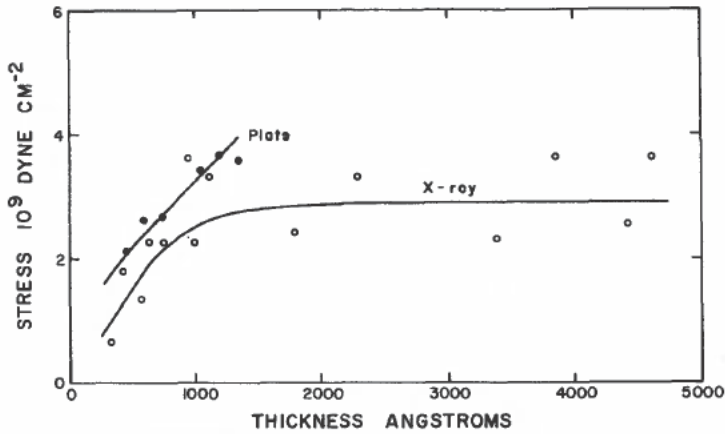
Fig. 8. Comparison of average stress in gold films by bending-plate and X-ray techniques. [Data from Kinbara and Haraki (46).]
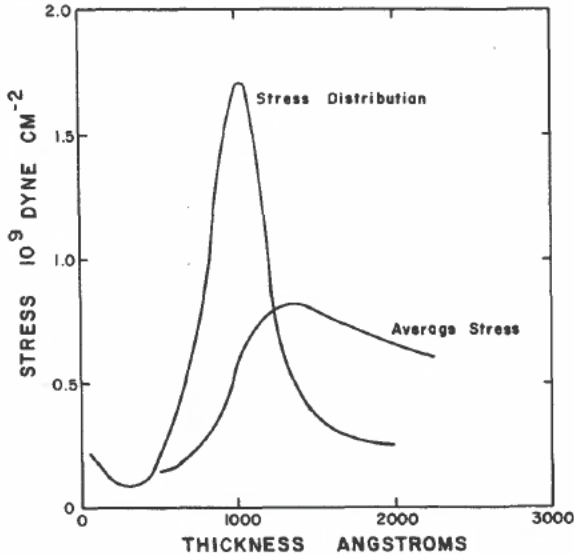
Fig. 9. Average stress and stress distribution for antimony. [Data from Horikoshi and Tamura (43).]

showed some saturation at the highest rates studied (70 A/sec). The Case laboratory, on the other hand, has not noted any strong effect for 20% rate changes about a mean of 60 A/sec in studying several transition metals, and Klokholm found no change in the 5 to 15 A/sec range for nickel.
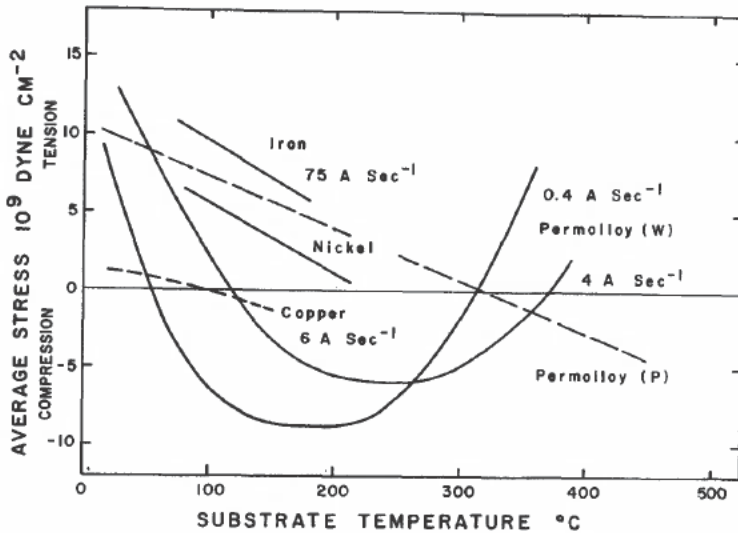
FIG. 10. Average stress as a function of substrate temperature. Permalloy (P) is total stress measured at room temperature after Prutton (58). Other data are intrinsic stress values. [Data: Permalloy (W), Weiss and Smith (51); copper, Horikoshi et al. (55); iron, Finegan (38); nickel, Hoffman et al. (63).

No systematic study of the effect of gas contamination on the stress in metal films has so far been published. Some large stress changes have been observed in films condensed in vacuum systems without cold traps, especially during the annealing of such films, but the stresses in films deposited in high-vacuum systems with a low-water-vapor content are not very sensitive to moderate changes in the residual gas pressure. It is thus not surprising that attempts have not been successful to correlate the observed scatter of stress data with residual gas pressure changes (32). There is, however, some evidence for the influence of the deposition atmosphere on film stress. Murbach and Wilman (27) found compression in aluminum films whenever the chamber pressure exceeded 10^{-4} torr during deposition, and they attributed this stress to oxide formation in the film. Halliday et al. (47) observed an increase in the compressional stress when copper films were aged in air at room temperature, and they actually saw the corresponding appearance of Cu_2O diffraction rings. Since the stress could be reduced considerably by etching the film, it seems that the stress was caused by the formation of a thin oxide layer at the film surface.

Values for the intrinsic stress in dielectric films are summarized in Table III. They are mostly taken from Blackburn and Campbell (30), Turner[2] (28),

[2]Turner, as well as Crittenden and Hoffman, has previously pointed out the practical importance of the connection between large tensile stresses and cracking in thicker films.

TABLE III

INTRINSIC STRESSES IN DIELECTRIC FILMS APPROXIMATELY 5000-A THICK

Material	Substrate temp., °C[a]	Substrate material	Stress, 10^9 dyne/cm²[b]	Sign[c]	Method[d]	Ref.
ZnS	110	Glass	1.0	C	C	30
	A	Glass	(0.022)	C	C	28
	A	Mica		C	C	60
SiO	110	Glass	1.2	C	C	30
	A	Nickel	4	T	C	33
MgF_2	110	Glass	2.0	T	C	30
	75	Mica	2.2	T	B	38
	A	Glass	(0.11)	T	C	28
	A	Mica	(0.11)	T	C	60
	A	Glass	1	T		57
LiF	110	Glass	0.4	T	C	30
	A	Cellulose	2.0	T	ED	47
	A	Glass	0.28	T		57
	A	Mica	(0.023)	T	C	60
	A	Glass	(0.023)	T	C	28
CaF_2	110	Glass	0.2	T	C	30
	A	Mica	(<0.0003)	T	C	60
	A	Glass	(None)		C	28
Cryolite	A	Glass	(0.061)	T	C	28
	A	Glass	(0.06)	T	C	60
	A	Glass	0.5	T		57
$PbCl_2$	50	Glass	0.18	T	C	30
	A	Glass	(0.014)	T	C	28
PbF_2	110	Glass	0.8	T	C	30
AgCl	A	Glass	(None)		C	28
AgF	A	Glass	(None)		C	28
AgI	A	Glass	(None)		C	28
BaF_2	A	Glass	(0.006)	T	C	28
BaO	50	Glass	0.15	C	C	30
Sb_2O_3	A	Glass	(0.004)	C	C	28
Sb_2S_3	A	Glass	(0.007)	T	C	28
Ce_2O_3	50	Glass	1.6	C	C	30
CeF_3	40	Glass	2.8	T	C	30
CdS	110	Glass	0.8	C	C	30
SnO_2	A	Glass	(0.008)	T	C	28
C	A	Glass	4.0	C	C	31
NaF	A	Glass	0.1	T		57
B_2O_3	90	Glass	0.1	T	C	30
Chiolite	A	Glass	(0.029)	T	C	28
AlPh[e]	40	Glass	0.6	C	C	30
MgPh[e]	40	Glass	0.6	C	C	30
MoO_3	A	Glass	(0.013)	T	C	28
CuI	A	Glass	(None)		C	28
AlF_3	A	Glass	(None)		C	28
$SrSO_4$	A	Glass	(None)		C	28

[a] A, thermally floating at ambient temperature.   [b] Values in parentheses are relative.

[c] C and T, compression or tension.

[d] B, end-supported beam; C, cantilever beam; and ED, electron-diffraction technique.

[e] Al and Mg thalocyanine.

Doi (57), and Heavens and Smith (60). Table III reveals two notable features. First, a relatively large number of dielectric films exhibit compressive stress even at low deposition temperatures, despite the relatively large film thickness, and, second, the many instances where the absolute value of the stress is extremely small. The stress values again do not include the Poisson term, but those from (30) are corrected for a Young's-modulus difference between film and substrate.

A laser interferometer technique has been developed by Ennos (60a) in which the substrate forms one mirror of a Michelson interferometer, allowing high sensitivity although vibrations of a half wavelength will cause the pattern to disappear. Data is given for the stresses in ZnS, MgF$_2$, ThOF$_2$, PbF$_2$, Cryolite, Chiolite, CaF$_2$, CeF$_3$, SiO, PbCl$_2$, TlCl, TlI, Ge, Te, CdTe, Al, and Cr.

Kinosita et al. (60b) report new data for MgF$_2$. ZnS. and Ag, ZnS may be tensile at slow evaporation rates, in contrast to previous work. A transition from compression to tension was noted at about 1200A, which could reflect the structure, or perhaps be a thermal effect. The new silver data does not show the hyperbolic average stress reported earlier (56).

The stresses in dielectric films show a more complex dependence on deposition parameters than do metallic films. Figure 11 shows the data of Blackburn and Campbell for the thickness dependence of the compressional stress in ZnS. The films have been evaporated at 20 A/sec on soft-glass beams held at 110°C. The curve indicates a large stress decrease with film-thickness increase. ZnS seems thus to behave considerably different than SiO. Priest and Caswell (33) found for films of the latter compound a relatively thickness-independent stress for the thickness range 1000 to 6000 A. The stress in ZnS films is similarly a strong function of the substrate temperature, while the stresses in SiO are not (Fig. 12). Figure 13 summarizes the stress dependence on the deposition rate for ZnS and SiO (B) according to Blackburn and Campbell and for SiO (P) according to Priest and Caswell. The stress differences shown may arise from the higher pressures used by Blackburn and Campbell, and from differences in source temperature. Indeed, Priest et al. (61) plotted the stress vs. the source power divided by the area of the tungsten filament (a measure of the source temperature) and found that the stress in SiO films was independent of the deposition rate, but a strong function of the source temperature. The oxygen partial pressure during evaporation is another important parameter determining the stress level in SiO films. Priest and Caswell observed an increase in tension when the concentration of oxygen was lowest, and Blackburn and Campbell's initially compression-stressed films similarly exhibited a decrease in compression for lower chamber pressures during deposition. According to Priest et al., films deposited at high partial pressures of water vapor or oxygen usually exhibit compression stress.
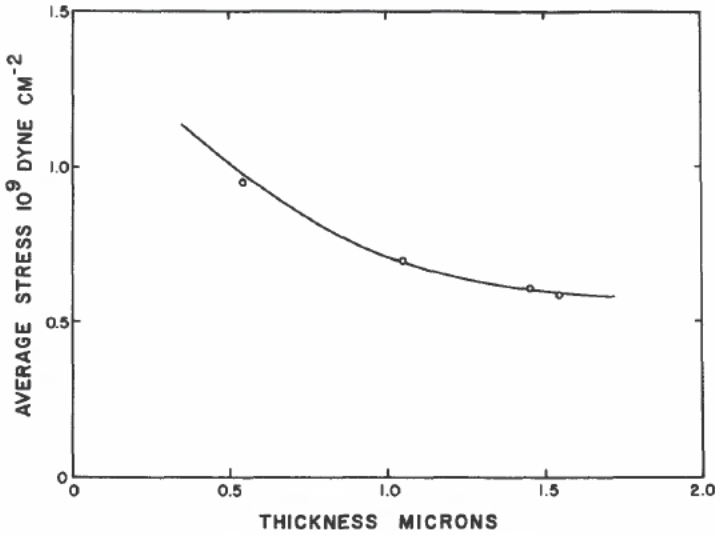
FIG. 11. Compressional stress in ZnS as a function of thickness. Data from Blackburn and Campbell (30) for substrate temperature 110°C; evaporation rate 21.5 A/sec.
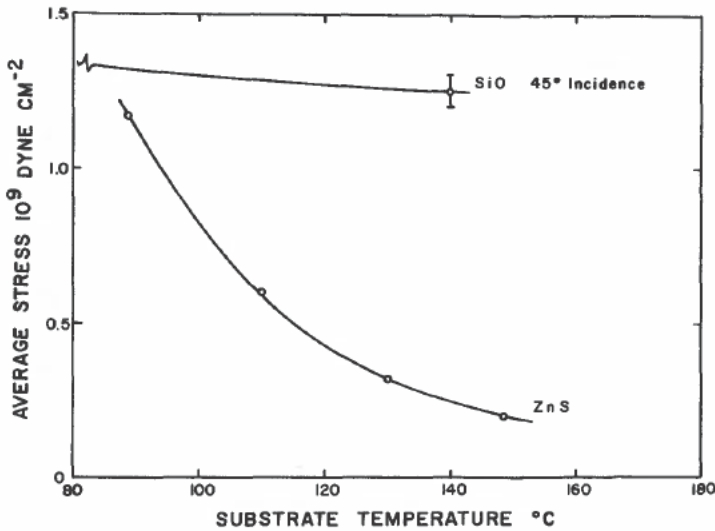
FIG. 12. Average compressional stress for ZnS and tensile stress for SiO as a function of substrate temperature. The SiO data from Priest et al. (36) extends to substrate temperatures of −125°C and is for 45°-angle-of-incidence films at source temperature of 1350°C. [ZnS data from Blackburn and Campbell (30).]

R. W. HOFFMAN
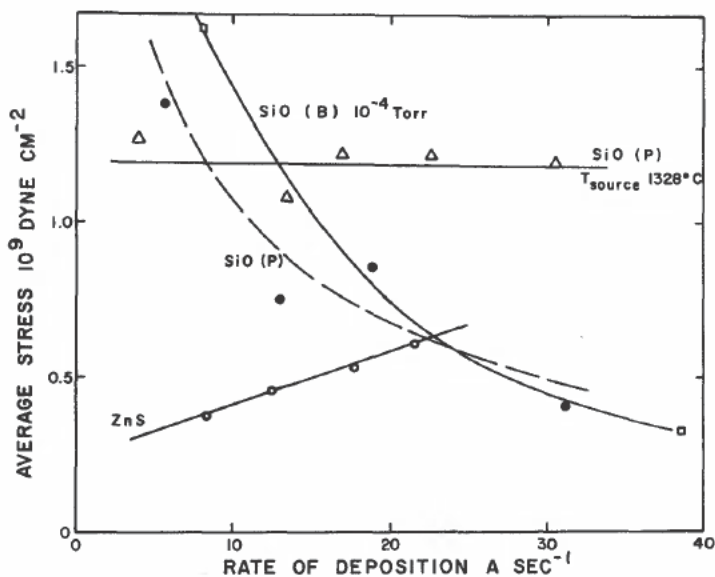
Fɪɢ. 13. Average compressional stress in ZnS and SiO (B) (30) and tensile stress in SiO (P) (33) as function of deposition rate. The difference in the SiO (P) data corresponds to changing the rate by varying the distance to the source or the source temperature. Compression is noted for SiO (P) at higher deposition rates.

Dielectric films may show a marked mechanical instability when exposed to air after their formation. This effect is accentuated when the evaporation is at other than normal incidence (36), and it presents a serious limitation to the use of SiO in evaporated circuitry and optical coatings. Priest et al. found for a 45° angle of incidence that the stress changed from 1.0×10^9 dynes/cm² tension to 1.0×10^9 dynes/cm² compression within 3 minutes after exposure to air, and that this stress change is often accompanied by buckling of the film from its substrate. These aging effects are caused by the partial pressure of water vapor, since no stress change was observed for exposure to dry nitrogen at atmospheric pressure. Evaporations at higher angles of incidence also result in pronounced anisotropies, which will be discussed later.

A detailed study of stresses in very thin LiF films has been published by Blackburn and Campbell (31). Their stress data for two deposition rates are reproduced in Fig. 14. For LiF films on carbon-coated glass substrates, the stresses have also been determined as a function of the average film crystallite size (15). This function indicates that tensile stresses are definitely present before the LiF film becomes continuous at about 100-A average thickness (Fig. 15). Halliday et al. (47) have shown that diffraction-line shifts observed on LiF are consistent with a cylindrical crystallite shape and an orientation of
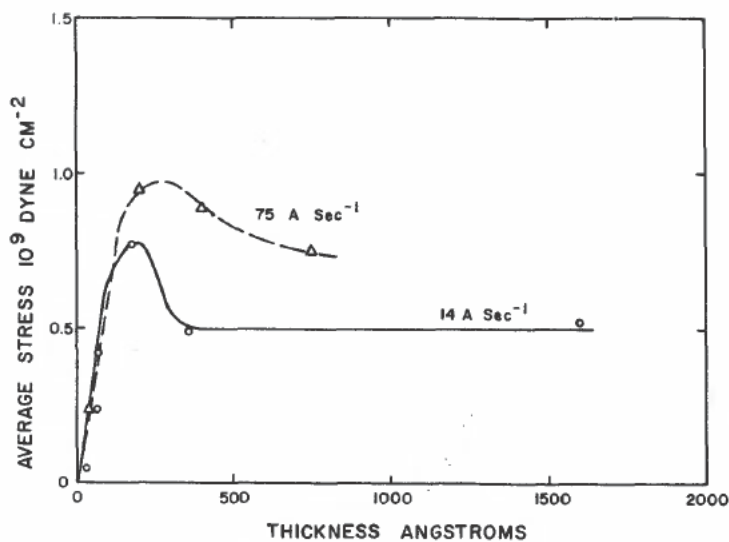
FIG. 14. Average stress of LiF as a function of thickness for two deposition rates. [Data after Blackburn and Campbell (31).]
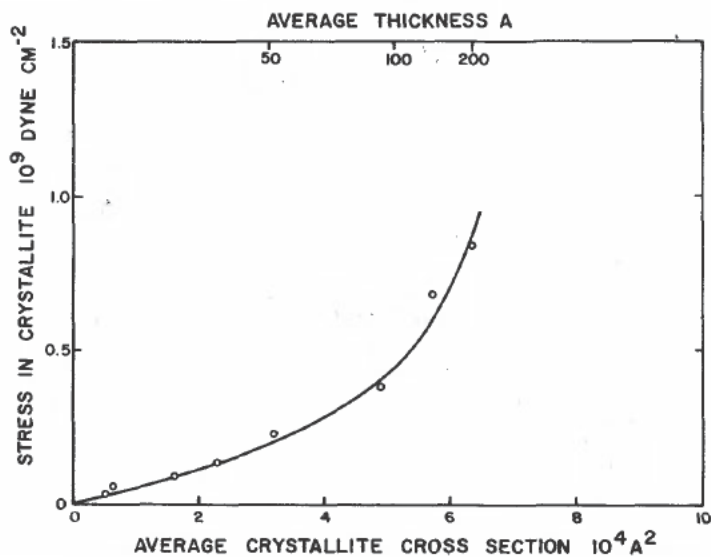
FIG. 15. Average crystallite stress in LiF as a function of crystallite cross section. Deposited at 12 A/sec on carbon-coated glass substrates. [From Blackburn and Campbell (31).]
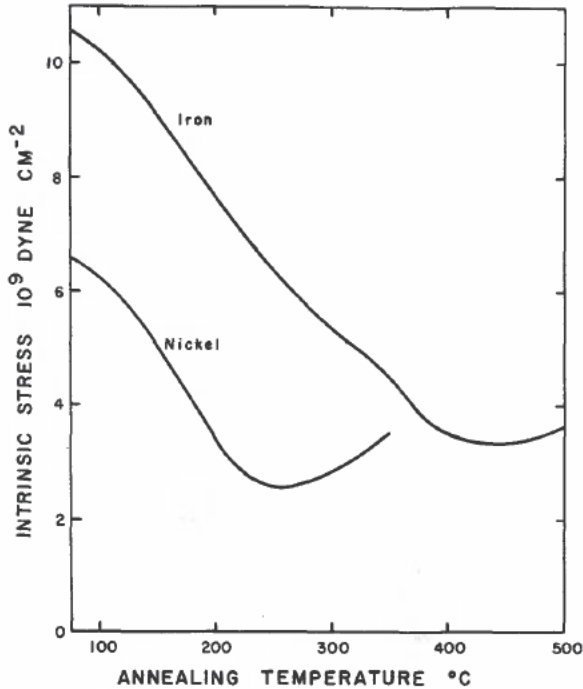
Fig. 16. Averaged data for intrinsic stress as a function of annealing temperature. [Data: nickel, Hoffman *et al.* (*63*); iron, Finegan (*38*).]

the cylinder axis normal to the substrate. The evaluation of the line shifts indicated further a negative surface tension of 1000 dynes/cm and internal stresses of about 5×10^8 dynes/cm^2. The latter were somewhat dependent on crystal size.

Since the internal stresses depend very much on the structural order of a film, it is interesting to observe their irreversible changes due to an extended anneal, where lattice defects are reduced and recrystallization proceeds. Figure 16 gives the change in intrinsic stress for 1500-A-thick iron and nickel films as a function of annealing temperature. The films were "pulse-annealed" in 25°C steps and 15-minute heating intervals, but they were always returned to the same base temperature for the stress measurement, to eliminate the influence of thermal expansion. Some annealing data for gold are shown in Fig. 17. They have been measured by Kinbara using both the plate (P) and the X-ray (X) method. The widely differing results between the X-ray and the deflection measurements indicate that recrystallization leads to a stress re-
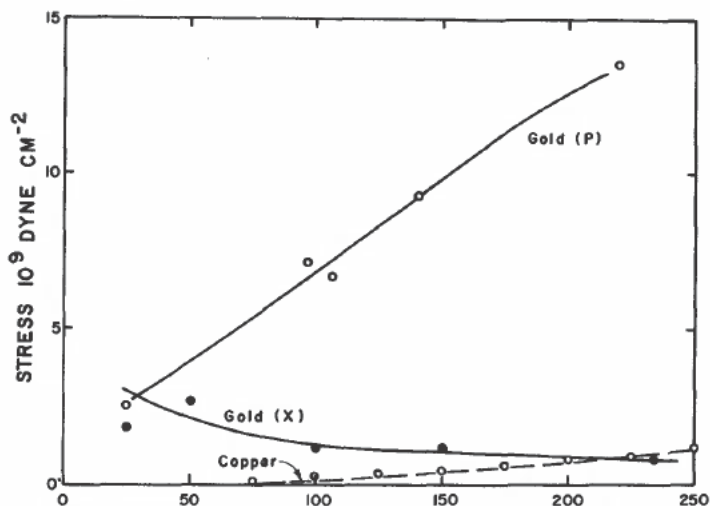
Fig. 17. Stress annealing in gold and copper. [Data: gold, Kinbara and Haraki (46) for X-ray (X) and circular-plate (P) experiments; copper, Hoffman et al. (63) and Story and Hoffman (32).]

duction within the crystal grains, but may increase the stress in the highly disordered grain-boundary areas which do not contribute to the X-ray line intensities. This stress contribution can evidently be so large that the over-all stress of the film increases. Davey and Deiter (62) also made stress measurements on gold films by X-ray diffraction. Their observations show a stress change similar to that observed by Kinbara, but of a somewhat smaller magnitude. The stress changes in nickel films during heating were studied by Hoffman et al. (63) for stress relaxation at the interface.

3. Models for the Origin of Internal Stress

A satisfactory theory for the origin of intrinsic stresses has yet to be formulated. The wide variation in the experimental results coupled with the lacking knowledge of structural details has led to a multitude of qualitative models. We shall review these models and discuss their successes and shortcomings, but before doing so, some practical cases shall be described where the thermally induced stress is the predominant contribution to the total internal stress.

a. Thermal Contributions. Thermal stresses are predominant in thin films of certain superconducting metals of low melting point such as indium, tin, and lead, when these films have been evaporated at room temperature and are subsequently cooled to the temperature of liquid helium. These films show no

intrinsic stress after formation ($<5 \times 10^7$ dynes/cm^2), presumably because they anneal rapidly enough at room temperature. Upon cooling, a biaxial thermal stress is generated. This stress is more complex than the one given by Eq. (10), since it exceeds the elastic limit of the film material and thereby induces plastic deformation. In the case of tin and indium, Toxen (64) and Blumberg and Seraphim (50) developed a model in which the maximum observable stress is limited by the critical shear stress arising from the pinning of dislocations at the surface. This gives rise to an expression of the form

$$\sigma = A + \frac{B}{t} \tag{11}$$

where A and B are constants related to the bulk shear stress and bulk shear modulus, respectively. The agreement is quite satisfactory for tin and indium, but Caswell et al. (65) found for lead that the values of B are appreciably larger than predicted by surface pinning, and that the observed stress is as much as four times larger than the theoretical thermal stress. Since surface tension effects were too small to account for this discrepancy, it is plausible
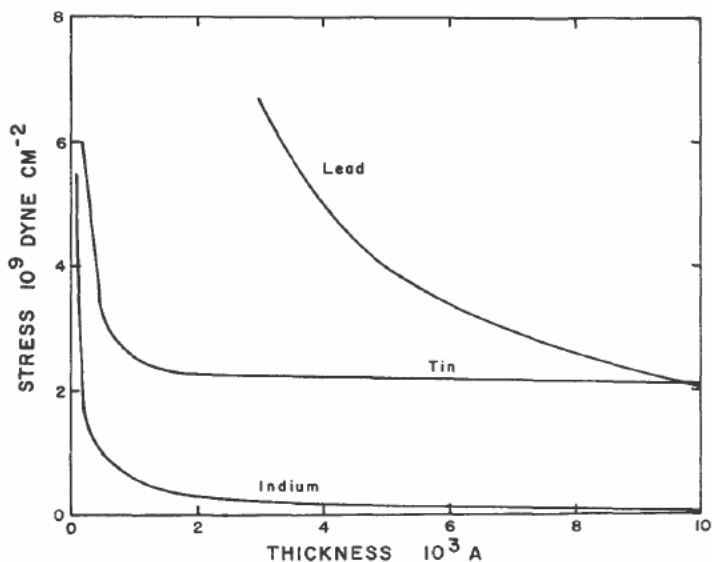
FIG. 18. Thermally induced stresses in superconducting films as a function of thickness. [Data: indium, Toxen (64); tin, Blumberg and Seraphim (50); and lead, Caswell et al. (65).]

to assume an additional dislocation locking mechanisms for lead. Some sensitivity to oxygen doping was also noted. Figure 18 summarizes the measurements of residual stress for typical low-melting superconductive films. Caswell *et al.* observed crystalline growth as a result of the large stresses induced by cycling the films to low temperatures. The growth offers a strain-relief mechanism and leads in the thinner films to the formation of holes. It should be noted that a similar growth has been proposed for whiskers (*66*).

A second example of predominantly thermal stresses has been found by Freedman in nickel films which have been grown epitaxially on rock salt at elevated temperatures (*48*). Since the expansion coefficient of rock salt is larger than that of nickel, the stress measured at room temperature was compressive. Freedman found that the stress was entirely elastic and could be relieved by floating the film free of the substrate. This result is consistent with Fig. 10, which indicates that the intrinsic stress in nickel films should be zero for deposition temperatures above 200 to 300°C. In summary it can be said that films of low-melting metals, as well as highly ordered films, show little if any intrinsic stress, and that under these conditions any apparent stress is caused by a differential thermal expansion between film and substrate.

Murbach and Wilman (*27*) have advanced the hypothesis that the total film stress might be explained as thermal if one regards the film surface during deposition as having a high temperature. The stress would then develop due to cooling from this high temperature according to the relation

$$\sigma = E\alpha_f(T_R - T_S) \tag{12}$$

where the hot surface temperature T_R should roughly equal the recrystallization temperature. T_S is the substrate temperature during deposition. Indeed the stresses in many metal films follow this relation, and the model accounts for the roughly linear decrease in stress as the substrate temperature is raised. Hoffman *et al.* (*63*) nevertheless question the validity of the hypothesis, because the thermal relaxation processes at the surface should be rapid enough to maintain the surface at approximately the substrate temperature. This contention is supported by Blackburn and Campbell (*30*), as well as by Pashley *et al.* (*6*), who showed experimentally that the condensing surface stays essentially at the substrate temperature, and that any heat pulse is rapidly dissipated. The thesis of a large temperature differential between condensing surface and substrates is also refuted by another observation. When films are raised, subsequent to their deposition, to a temperature higher than the deposition temperature, they exhibit the irreversible changes of a typical annealing process, indicating that no part of the film was previously exposed to such a higher temperature.

b. Amorphous-Crystalline Phase Change. There is no question that phase transitions in films should lead to corresponding changes in stress, since they

are always accompanied by a change in volume. This has been illustrated for the case of Sb. Polymorphic changes have not been reported but might be of particular importance for semimetals and at very low substrate temperatures.

c. Surface Layers. Halliday *et al.* (*47*) report that the compressive stress in copper films increases with the growing thickness of a surface oxide layer, and decreases when the oxide is chemically thinned. This stress dependence on surface oxidation is not surprising and has been observed repeatedly. Reisenfeld (*67*), for instance, has noted a 30% increase in the stress of iron films after a 15-minute heating in air at 100°C. A very thin surface oxide layer might also explain the about 10-A-thick stress layer deducted by Kinosita and Kondo from the hyperbolic relation they observed between stress and film thickness. Highly strained or pseudomorphic layers at the substrate interface, of course, would similarly give rise to a stress which is independent of the film thickness.

Gimpl *et al.* (*19a*) finally suggest that amorphous layers might be found at both metal film surfaces, an assumption which is supposed to account for the high strength often measured on films. These amorphous layers are probably oxides which are responsible for most of the observed stress, since the body of the film should exhibit nearly the properties of the bulk metal and should thus relieve higher stresses by plastic flow.

d. Interfacial Dislocations. Van der Merwe (*68–71*) has shown that epitaxial films can reduce their total energy by forming interfacial dislocations which decrease the lattice misfits at the expense of introducing an elastic strain into the film. A derivation of this minimum-energy state resulted in a complicated function depending on the degree of misfit, strength of the interfacial bonding, and the elastic properties of substrate and film. This model has been developed for a one-dimensional lattice misfit only.

As a consequence of Van der Merwe's theory, dislocation-free films can only exist when their thickness and substrate-lattice misfit stay below given threshold values. Thus, for a given misfit below the critical or threshold value, a relatively thick deposit might be obtained which is strained to match the substrate lattice without interfacial dislocations, but for misfits greater than the misfit threshold, interfacial dislocations always occur for even a monolayer film. The critical misfit values can be as large as 13% for a "soft" film with "strong" bonding to the substrate. "Hard" films with a "weak" bond, on the other hand, may have a critical misfit value of only 0.04%.

Only Matthews (*72*) has so far checked experimentally the theory of Van der Merwe on epitaxial films. His observations on 450-A-thick PbS films grown on PbSe and PbS crystals not only show the predicted dislocations by diffraction contrast, but an elastic strain of 0.06%, which agrees precisely with the theoretical value. This confirmation of Van der Merwe would be more persuasive, no doubt, if it would be supplemented in the future by measurements on films with large intrinsic stress values.

There is, unfortunately, little agreement between the large body of experimental stress and strain data obtained on polycrystalline films and the theory under discussion. For one, experimental evidence does not verify the prediction that the homogeneous strain should vary inversely with film thickness. Second, tension or compression should be observed depending on the condition of a positive or negative misfit, whereas most experiments show tension film stress regardless of the sign of the misfit. Finally, there is little quantitative agreement between predicted and measured stress values. It is probably not surprising that the theory of Van der Merwe breaks down for polycrystalline films, since the fine structure of the substrate surface has in this case little influence on the film growth.

Van der Merwe also predicts that the stress and strain imposed by the substrate-film interface decrease exponentially with the distance from this interface, and Klokholm (52) has checked this prediction experimentally.

e. *Defect Models.* Concurrent changes of stress and electrical resistivity in nickel and copper films (32, 73, 74) during pulse annealing suggest that the intrinsic stress is related to point defects and defect clusters. A semiquantitative treatment has been given for single vacancies and interstitials migrating to a free surface. The out-annealing of vacancies leads to a stress reduction above room temperature. Typical stress and resistance changes in annealing copper films are reproduced in Fig. 19. The activation energy for the anneal of mobile defects in films (75) compares closely to that required to heal radiation damage and cold-work defects in bulk-material [see Van Bueren (76) for a summary],
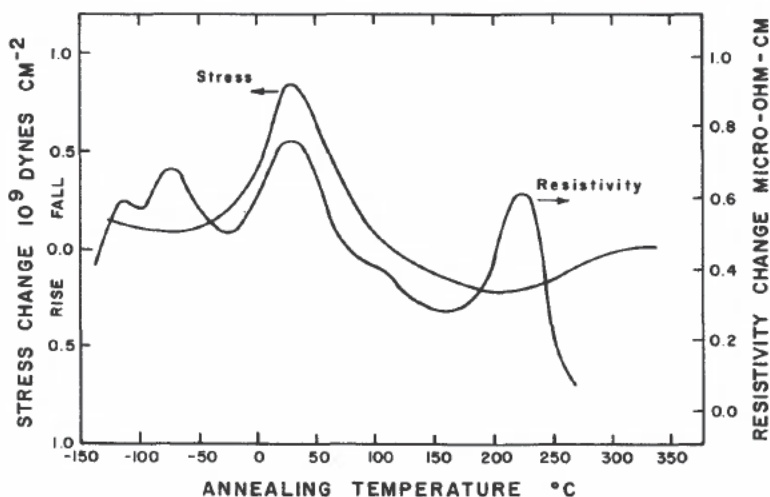
FIG. 19. Correlation of stress and electrical resistivity changes of copper films during "pulse anneal" treatment. [Data from Story and Hoffman (32).]

but the annealing kinetics are too complex for a detailed analysis. The total stress relief at room temperature corresponds, according to Story and Hoffman, to a loss of about 1 % vacancies. There can be no question, however, that the point-defect model is too great a simplification to account fully for the stress behavior in films. If, for instance, an appreciable amount of vacancies migrates to the inner grain boundaries, the stress increases, and this might mask or at least reduce the stress reduction due to a vacancy migration to the free surfaces. Another process competing with the release of point defects to the film surface is the considerable recrystallization which, according to Keith (77), often takes place in the same temperature range.

Rymer (78) has attempted to determine the actual stress pattern in aluminum and gold films by a sophisticated application of electro-diffraction techniques, where he evaluated the interplanar spacings as well as the line profiles. The results could be interpreted as representing a homogeneous triaxial stress system, but the most probable explanation was obtained by assuming an inhomogeneous strain arising from stacking faults and dislocations. In a later study on silver films, Rymer et al. (79) found also the presence of stacking faults and an inhomogeneous stress pattern, and in this case they attributed the observed line broadening definitely to the presence of random strains and not to a small crystallite size.

X-ray or electron-diffraction line breadth may indeed be used to obtain the microstrain as well as the particle size. Although several authors have used these techniques, insufficient emphasis has often been placed on a separation of the two contributions. Halteman (80), however, has shown that the line broadening in a 50-A nickel film resulted from microstrain alone. He obtained this result by analyzing the change in line broadening with Bragg angle as well as the Fourier transforms of the line slopes. Bacon (81) found by similar measurements on thin nickel films, that the microstrain decreases during anneal in much the same way as the macrostress. More recent line-breadth measurements have been made for permalloy and nickel films by Smith (82) and Segmüller (83, 84).

f. Surface Tension. As outlined by Heavens and Smith (60), Halliday et al. (47), and Caswell et al. (65), surface tension can be an important contribution to the stress of thin films. Given a film with no other stress terms than the surface tension τ_1 at the film-vacuum interface and τ_2 at the film-substrate interface, then the total apparent stress can be written

$$\sigma = \frac{\tau_1 + \tau_2}{t} \tag{13}$$

A positive surface energy manifests itself as tension in a bending-plate experiment and as a reduced lattice constant in X-ray or electron diffraction. A short calculation shows that a realistic surface energy of 1000 ergs/cm^2 yields for a

1000-A-thick film a stress of only 2×10^8 dynes/cm^2. Since this is about one order of magnitude smaller than the total stress measured on a typical film of this thickness, one can safely conclude that the surface tension is only a minor factor in the stress behavior of films.

The effect of the surface tension, however, might not be small when the film consists of small isolated crystals. An increased interatomic spacing is an indication of a negative surface energy, and Rymer (85) has indeed shown that small LiF crystallites have a larger lattice constant, in agreement with his prediction about the surface energy of LiF.

An extension of the surface-energy model has been proposed by Smith et al. (11) by considering the reduction in surface energy when two (spherical) crystallites coalesce. The crystallites are prevented from doing so by bonding to the substrate. In a more recent paper, Weiss and Smith (51) suggest that the tension observed under certain conditions in permalloy films results from the coalescence of grains, whereas the compression stress of samples prepared under different conditions is caused by the surface tension of the individual grains. More precisely, the sign of the film stress is supposed to depend on the balance of the two effects. The authors observed that the transition from tension to compression shifted toward higher temperatures when faster deposition rates were employed, and they explained this effect as being caused by the reduction in grain size due to the rate increase.

g. *Crystallite Boundary Relaxation.* The previous sections showed that quantitative models for the intrinsic stress followed from the approaches by Murbach and Wilman or Van der Merwe, but that the contributions of surface tension and lattice defects could only be discussed in a qualitative manner. Finegan and Hoffman (44) have attempted to construct a more detailed quantitative model by including the consideration of surface tension and growth processes at the grain boundaries, based on their observations of iron films. A somewhat simplified model of film formation is assumed in which the nuclei grow first as hemispheres until they touch, and subsequently as columns with densely packed boundaries. The interatomic forces at the boundaries tend to close any existing gap, with the result that the neighboring crystallites are strained in tension.

During the very first nucleation stage, each nucleus is strained only by its surface tension, but can migrate quite freely over the substrate surface until it reaches a radius where the bonds of the iron atoms to the surface freeze due to the strains imposed by the surface tension. This anchoring of the crystallites occurs for iron at a radius of about 10 A, and it induces the first measurable strain into the substrate. The contraction of a 10-A-large crystallite due to the surface stress is of the order of 1 %.

The next phase, represented by the further growth of the anchored, but still isolated nuclei, is characterized by an expansion of the crystallite lattice

due to the decreasing influence of the surface tension. This lattice expansion, in turn, induces a bending of the substrate that indicates film compression. An iron crystallite of 60 A exhibits on a 75°C substrate a contraction of about 0.35 A, or about a quarter of the contraction of a 10-A nucleus, if data from Pitsch (86) are extrapolated. Thus, a force-thickness curve determined by a bending-plate experiment exhibits no stress up to an island size of the order of 10 A, but has a region of increasing compressional force up to the point where the islands touch and grow together. Such behavior is indicated schematically in Fig. 20. As the grains begin to form a continuous layer, many
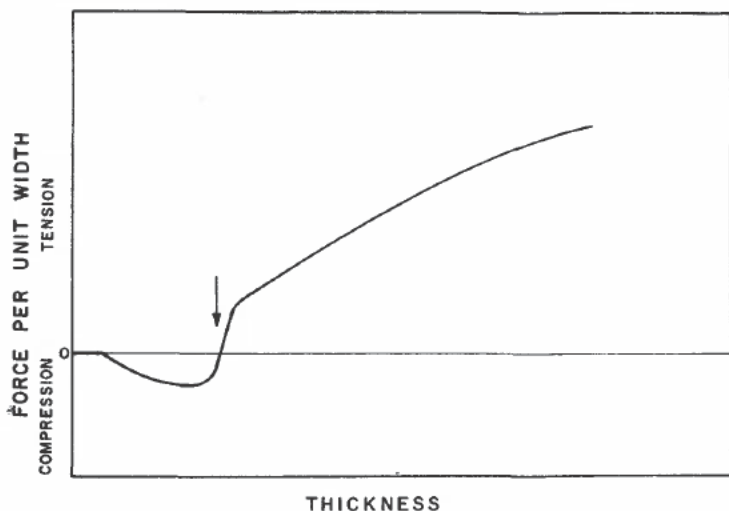
THICKNESS

FIG. 20. Schematic representation of force per unit width following composite surface tension—crystallite mismatch relaxation model. The thickness indicated by the arrow corresponds to the film becoming continuous.

unclosed gaps still exist between the crystallites. A detailed analysis shows that the closing of these gaps results in a sharply increasing tensional stress. After the film has reached a sufficient thickness so that it has passed through this transitional stage, it reaches an average strain value equal to the average atomic relaxation distance $\bar{d}$ divided by the average crystallite dimension l. The corresponding stress can then be given as

$$\sigma_x = \frac{E}{1 - v_f} \frac{\bar{d}}{l} \tag{14}$$

To evaluate this formula, Hoffman constructed an average interatomic force

which follows Hooke's law for small displacements and decreases exponentially for large displacements. For iron he obtained an average mismatch relaxation of about 0.55 A, if the surface tension is neglected. For the case of increasing crystal size during film growth, the stress increases more slowly than linear, as indicated in Fig. 20.

This model shows reasonably good agreement with typical experimental results. It exhibits a force per unit width which increases about linearly with thickness and a nonzero intercept when stress data for thick films are extrapolated to zero thickness. It also permits a qualitative consideration of the effect of condensation rate and substrate temperature on nucleation and crystallite size. The model yields little or no stress for single-crystal films, and even indicates a small intrinsic stress for polycrystalline films with large grains. It does not, however, account for a compressive intrinsic stress except in the early stages of growth, when the film is still discontinuous. It thus offers no explanation for the permalloy data of Weiss and Smith in the low-temperature range, or for the linear stress decrease with increasing temperature shown in Fig. 10. The constant-stress data of Klokholm are hard to explain, since the crystallite size ordinarily changes as the film builds up and should thus lead to a corresponding change in stress.

There seems to be no definite evidence for compression stress in metal films of the island stage. It should be considered, though, that compression is not easily distinguished from the thermal effects, owing to radiation heating of the substrate during a run. For materials with a negative surface tension such as LiF, the island stage should exhibit tension and not compression, followed by a steep rise in the tension when the crystallites grow together. The data of Blackburn and Campbell shown in Fig. 15 verify this expectation.

One additional feature is worth mentioning. Most metal firms curl in a concave manner when removed from the substrate. Any model which develops a higher tension near the film-substrate surface than at the free surface will not account for this observation unless an additional oxidation layer at the free surface is involved.

The annealing experiments can be understood to some extent. An increase in crystallite size, coupled with sufficient diffusion along the grain boundaries to account for any volume change, must lead to a decrease in stress as is generally observed. The stress increases observed for gold and copper between 100 and 200°C and for nickel at higher temperatures, however, can only be explained by this model, if one assumes that the transport of material by diffusion is too small to counteract the volume change. The quantitative aspects of this model of combined surface tension and crystallite relaxation have clearly not been examined in sufficient detail, especially not for the early growth phases.

4. Anisotropic Stress

So far both the experiments and the models have been concerned with an isotropic intrinsic stress. There is evidence that anisotropic stresses also exist in films when the atomic beam arrives during deposition at an angle oblique to the substrate surface. Anisotropic stresses are also expected from differential thermal expansion when films are condensed on low-symmetry single-crystal substrates. The circular-plate technique lends itself to the observation of stress anisotropies, but Priest *et al.* (*36*) have shown that orthogonal cantilever beams can also be used. Behrndt (*86a*) has found qualitative evidence for anisotropy in obliquely deposited ZnS films by interpreting the symmetry of the stress patterns which developed when the films were exposed to air.

a. Summary of Experimental Results. The angle of incidence for oblique depositions is given by the evaporant beam and the substrate normal. The plane determined by these two lines is called the plane of incidence. The direction in the film plane perpendicular to this plane of incidence is designated as the x direction; the y direction is then the intersection of the two planes, and as such perpendicular to x. With this notation, the stress anisotropy can be defined by a graph of σ_x and σ_y, or better by giving the ratio σ_y/σ_x.

Data for σ_x and σ_y of iron films deposited at 36.5° incidence have been given in Fig. 5 as a function of film thickness. Values of the stress ratio for iron (*41*) and SiO (*36*) are presented in Fig. 21 as a function of the angle of incidence. The stress is isotropic for normal incidence in both cases. Iron exhibits a stress ratio which decreases roughly as the cosine of the angle of incidence, but SiO shows a more complex behavior.

Cohen *et al.* (*87*) report circular-plate experiments in which a large anisotropic strain was found, but attributed most of this to nonuniformities in the substrate and concluded that the stress was isotropic. Smith *et al.* (*11*), on the other hand, have deduced a strain anisotropy in obliquely deposited permalloy films from the change in magnetic anisotropy which occurred upon stripping the films from their substrates. They found the same sense of anisotropy as the one reported for iron, and with about the same magnitude.

When iron films are pulse-annealed, it is observed that the stress ratio decreases monotonically with temperature (*67*). The equivalent change in force per unit width is shown in Fig. 22 for 15-minute anneal steps up to 200°. It can be seen that the stress reduction is always largest in the y direction. It should be noted that the F_x curve changes its slope during anneal, but not its intercept with the zero-thickness coordinate, whereas F_y shows just the opposite behavior. Moreover, the x and y intercepts yield different zero-thickness stresses. These features are not understood at present.

b. Models for Anisotropic Stress. Smith *et al.* suggested that the anisotropy arises during film growth from a random nucleation in combination with a
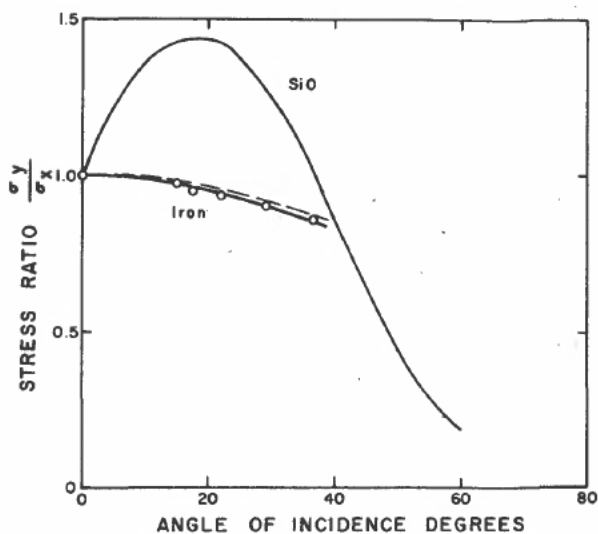
FIG. 21. Stress ratios for iron and SiO as a function of angle of incidence. SiO after Priest *et al.* (*36*), iron from Finegan and Hoffman (*41*). The dashed curve is calculated on the basis of a cosine dependence for the strain.
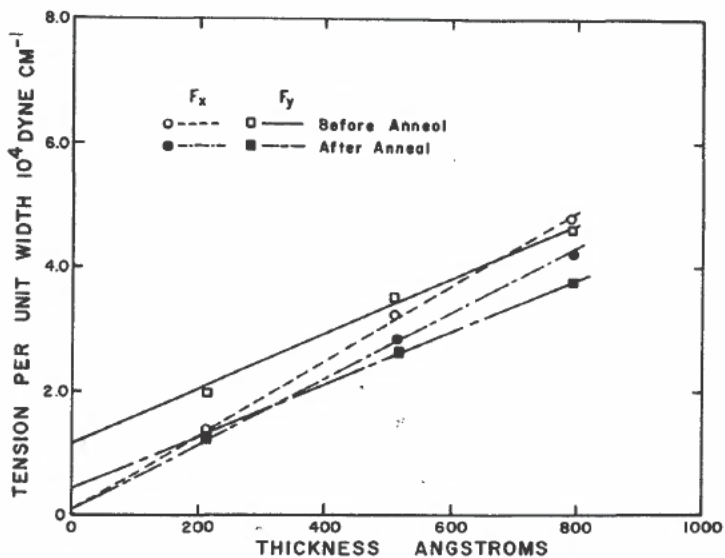
FIG. 22. Force per unit width changes after anneal to 200°C for iron film at 36.5° incidence. [From Riesenfeld and Hoffman (*67*).]

self-shadowing effect for other than normal incidence. This model leads to the formation of chains of crystallites perpendicular to the plane of incidence, and the resultant surface-tension pattern might combine with substrate constrains to yield the observed stress anisotropy. Evidence for chain formation was obtained by electron microscopy for very thin films, and by resistivity and optical measurements for thicker films. Priest *et al.* found no evidence for self-shadowing until the angle of incidence was greater than 45°.

Finegan and Hoffman suggested that anisotropic nucleation could also play a role, since nuclei might be slightly farther apart in a direction parallel to the plane of incidence. The displacement giving rise to the strain would thus be spread over a larger distance, resulting in a smaller strain in the y direction. The dotted curve in Fig. 21 is calculated on this basis and is in approximate agreement with the experimental data.

To fit the data in Fig. 22 also, it was proposed by Riesenfeld and Hoffman (67) that the stress anisotropy is caused by a combination of anisotropic nucleation and anisotropic film growth. The resultant growth pattern is shown schematically in Fig. 23. Since the grains become, during growth, elongated in the x direction, the surface tension of the grains induces a compressive σ_x larger than σ_y. During the further growth of the film, the islands join first in the x direction, and only distinctively later in the y direction. In the fully developed continuous film, however, the crystallites are largest in
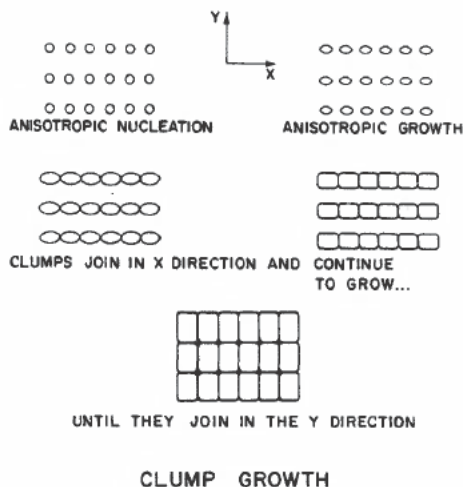
FIG. 23. Representation of anisotropic nucleation and growth of angle-of-incidence film.

the x direction, and consequently have more boundaries per unit length in this direction. Such a growth pattern should yield a greater slope for F_x, as well as an intercept which depends on the relative magnitudes of the compressive and tensile contributions to the stress. (This ratio of compressive to tensile stress, in turn, follows from the shape of the grains when they just touch.) The small intercept for the F_x curve in Fig. 22 implies then for very thin films a larger compressive contribution to the stress in the x orientation and the steeper slope of F_x indicates a higher concentration of crystallite boundaries in the x direction. The growth model of Hoffman and Riesenfeld thus seems consistent with the experimental data shown in Fig. 22. The fact that the F_x and F_y curves approach each other during anneal indicates that the crystallites as well as the film as a whole become more nearly isotropic, a fact which is to be expected.

IV. Tensile Properties

Ever since early observations have indicated that thin films are "stronger" than bulk, there has been much interest in the tensile properties of films. The experimental techniques used, the important experimental results, and present theoretical models will be discussed in the next section. Unfortunately, widely varying results have been obtained in different laboratories, and the models offered so far are just about as numerous as the experimental observations. The picture is in one aspect simpler than that of stress measurements, however, since the tensile properties are not so much influenced by the crystallite size.

1. Experimental Techniques

a. High-Speed Rotor. The first measurements were made by Beams and his collaborators (*88*). They electroplated the films to be measured directly onto rotors which were subsequently spun at high speeds. This approach eliminated any mounting problem, but restricted the observation to the ultimate strength only. The adhesion of the film to the rotor must be carefully controlled for a reliable measurement of the film strength. Since this method does not yield a stress-strain curve and requires rather specialized equipment, it is not in general use for tensile measurements.

.b. Bulge Test. To surmount the mounting problem and obtain the stress-strain curve, Beams (*89*) and others (*90, 91*) have used the bulge test, where the film is mounted on the end of a hollow cylindrical tube and pressurized. In some cases, a plastic film is mounted over the end of the tube, and a metallic film is then evaporated on the plastic substrate. The substrate is dissolved prior to pressurizing. In another approach a hole was drilled through the substrate to provide direct pressure access to the film, thereby avoiding

any handling of the film. The biaxial stress of the film can be calculated from the pressure, and the strain from the center deflection of a deformed specimen according to

$$\sigma = \frac{Pr^2}{4tD} \qquad \varepsilon = \frac{2}{3}\frac{D^2}{r^2} \tag{15}$$

where P is the pressure difference between the two sides of the film, r the internal radius of the tube, t the film thickness, and D the height of the center of the bulged film above the end of the tube. The deflection is observed by a microscope or optical-interference techniques, and it is assumed to be approximately hemispherical.

As we know from the previous sections, an initial stress may be present. Cabrera (89) has shown that σ in Eq. (15) should be replaced by

$$\sigma = \sigma_0 + \frac{2}{3}\frac{E}{1 - v_f}\frac{D^2}{r^2} \tag{16}$$

if the initial stress at $D = 0$ is σ_0. He has also worked out a more exact theory, but, according to Beams, the, measurements are not sufficiently accurate to warrant its use. If the gauge pressure is plotted against the bulge height D, the initial stress may be determined from the slope of the first few points, a procedure which of course assumes elastic deformation only. Values of σ_0 are about 10^9 dynes/cm^2 and fall thus into the range of the intrinsic stress values as measured by previously discussed methods. Rectangular bulges have been used with no apparent difference in behavior.

Papirno (92) has suggested that the bulge surface is better described as a general quadratic surface of revolution than as a hemispherical surface. He obtained an empirical relationship for the strain, varying as $0.30 \ (D/r)^{1.9}$ rather than $0.67 \ (D/r)^2$, a value which would follow from a hemispherical approximation. Thus the strains observed in bulge experiments may be in error by more than a factor of two.

c. Microtensile Testing Machines. Many different microtensile testers have been built for the observation of the small loads and elongations typical of thin-film work. "Soft" types are those in which the load is given and the elongation is measured, whereas "hard" types prescribe the strain rate and measure the load. In thin-film studies, soft machines are more common. Corrections for machine hardness have not always been made in published studies, and nominal stress-strain curves have mostly been reported in which the changing cross section of the film was neglected.

In the soft category, Marsh (93) has developed a null torsion balance which applies the force. The extension is measured from a mechanical linkage with a sensitive optical null detector permitting the determination of elongations greater than 5 A. Neugebauer (94) and D'Antonio et al. (95) have applied

the uniaxial load by use of a solenoid magnet. The elongation was measured to 0.2 μ by direct observation of the motion of the loading rod through a microscope. Oding and Aleksanyan (96) have used a gravity-loaded cart on an inclined plane. Blakely (17) has described a soft machine in which the beam is loaded electromagnetically, and the strain sensed by an interferometric method.

Various hard machines have also been described. Kuhlmann-Wilsdorf and Raghavan (97) have constructed a microtensile machine that uses a strain-gauge-proof ring to measure the load, and a differential transducer for measuring the elongation. Lawley and Schuster (98) have also constructed a tensile machine in which the stress is measured by a load ring sensed by a differential transformer while the strain is observed optically. Blakely uses a load cell of etched-foil strain gauges, operating at a strain rate of 0.2% per minute. It is suggested that the original papers listed in Table IV be consulted for details.

TABLE IV

TENSILE-TEST APPARATUS

Type	Stress	Strain	Ref.
High-speed rotor	Angular velocity		88
Bulge	Gas pressure	Microscope	87
Bulge	Gas pressure	Interferometer	90
Bulge	Gas pressure	Interferometer	91
Soft	Null torsion balance	Null optical lever	93
Soft	Electromagnetic	Differential transducer	94
Soft	Electromagnetic	Optical microscope	95
Soft	Inclined plane	Optical	96
Soft	Electromagnetic	Interferometric	17
Hard	Strain gauge	Differential transducer	97
Hard	Load ring-differential transducer	Optical	98
Hard	Strain gauge	Motor drive	17

Common to all the methods is the difficulty of mounting the film in such a way that uniform loading can be obtained without tearing the film at the edges. The measurements are hardly reproducible, and many films are found with low strength, presumably as a result of either rough handling, poor mounting, or large-scale defects in the films themselves. The shape of the

specimen is of some influence. Orowan grips (99) reduce the stress on the edges of the specimen, but do not provide an easy calculation of the nonuniform stress. Even so, a rumpling of the film is almost inevitable and can invalidate the results (100). Ordinary grips give a uniform stress, but may result in "overstraining" of the damaged edges. Conventional tensile-test-shaped specimens have been cut from a free film or evaporated through a mask (101). Lawley and Schuster (98) use a photoengraving technique to cut a long sample from a rolled foil to avoid tears or cold-worked edges. Most of the other workers use a rectangular sample narrower than the grips, and with a gauge length of a new millimeters. D'Antonio et al. (95) have taken advantage of the nonuniform internal film stress. They let the film roll into a scroll after removal from the substrate and glued the resultant tube with epoxy cement to the grips. This geometry allows handling of the specimen with greater ease and avoids some of the tearing and alignment problems. Neugebauer (94) has first glued the films to the grips and then removed the film from the substrate, thereby avoiding any rough handling of the film. Kuhlmann-Wilsdorf and Raghavan (97) hold the film by friction in a set of corrugated grips. Marsh (93) has used a flotation method to raise the film to the grips.

The details of the stress-strain curves can depend on the initial film stresses, on damage caused by the mounting of the film, and on any creep which might occur in the mounting cement. To avoid damage by surface tension Blakely (17) has left, during testing, the specimen immersed in the brine used to dissolve the NaCl substrate. Tensile testing of thin films is especially sensitive to bending of the film; hence careful alignment of the grips is essential. If all precautions are taken, the specimen usually fails within the gauge length, giving some confidence that the grips have not damaged the film to a critical extent.

   d. Electron-Microscope Devices. Wilsdorf (102) has built a fixture which permits the straining of foils in the electron microscope at a constant strain rate, and he has applied this technique in a detailed study of dislocations in rolled aluminum foils. Pashley (103) also has described a technique for straining the specimen while observing it in the electron microscope, but accurate values of both stress and strain are difficult to measure. Since the film is mounted over a wedge-shaped slit and the wedge is opened during the test, a nonuniform strain is applied to the sample. Pashley found for gold an elastic behavior with fluctuations which might have been caused by true changes in the specimen or by shortcomings of the mounting, but Palatnik et al. (104) observed a smooth strain curve. In both cases fracture was accompanied by a sharp change in the diffraction pattern.

2. SUMMARY OF EXPERIMENTAL RESULTS

The tensile properties of films have been reviewed by Menter and Pashley (100), Hoffman (105), and Neugebauer (2). The data reported so far are not

very consistent. Single-crystal gold films have been studied by the Tube Investments Laboratory (*100, 106, 107, 108*), and by Catlin and Walker (*90*). Neugebauer (*94*) and Blakely (*17*) have reported results for single-crystal gold films and for polycrystalline gold films with various orientations. Beams *et al.* (*88, 89*) have studied polycrystalline gold and silver films. Polycrystalline silver has also been investigated by Palatnik *et al.* (*104*). Palatnik and Il'inskii (*101*) and Oding and Aleksanyan (*96*) have studied polycrystalline copper films, whereas Lawley and Schuster (*109*) measured copper foils prepared from rolled material. Nickel prepared by evaporation was investigated by D'Antonio *et al.* (*95*), cold-rolled, electroplated, and chemically deposited nickel by Jovanovic and Smith (*91*). Aluminum films were measured by Palatnik *et al.* (*104*). References (*89, 90,* and *91*) used the bulge test, (*104*) electron defraction, and all others microtensile testers.

A typical stress-strain curve according to Neugebauer is shown in Fig. 24.
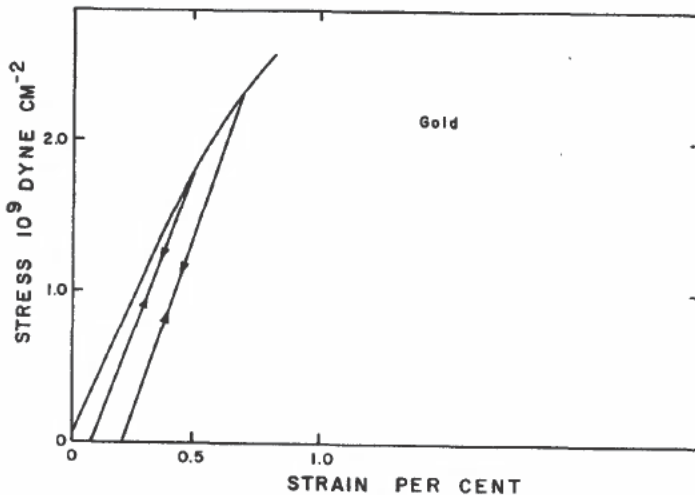
FIG. 24. Typical stress-strain curve for thin film. [After Neugebauer (*94*).]

Most workers find an irreversible initial loading curve, but almost reversible unloading and reloading as long as the previous level is not exceeded. The slope of the initial loading curve is smaller than the slope of the unloading curve. The change in slope has been attributed to an elastically soft measurement or to creep in the sample or cement, but it is most likely that the non-elastic behavior is attributable to the film itself.

a. Elastic Modulus. Values of the elastic-modulus have been calculated from the unloading data and are summarized in Table V, along with creep

observations. Neugebauer concluded from his measurements that the modulus of gold films has the normal bulk value. Catlin and Walker also report excellent agreement with the elastic modulus of bulk gold for (100) films at film thicknesses greater than 4000 A, but an increase in the modulus is noted for the thinner films. The work summarized in (89) seems to be the only data to indicate a thickness-dependent elastic modulus.

TABLE V

ELASTIC AND CREEP PROPERTIES

Material	Structure	Test	Modulus	Creep observed	Ref.
Au	(111) crystal	Tensile	Normal	[a]	100
	(100) crystal	Bulge	Thickness dep.	Short-term	90
	(100) and (111)	Tensile	Normal	Yes	94
	Polycrystalline	Tensile	Normal	Yes	94
	Polycrystalline	Bulge	High	Yes	89
	Single and polycrystalline	Tensile	Normal	Yes	17
Ag	Polycrystalline	Bulge	High	Yes	89
	Polycrystalline	Electron diff.	Assumed normal		104
Cu	Rolled foil	Tensile	Normal	Yes	109
	Polycrystalline	Tensile	Normal	Yes	96
Ni	Polycrystalline	Tensile	Normal	Yes	95
	Amorphous chemical deposit	Bulge	Low	No	91
	Electrodeposited	Ewing's method	High		110
	Aluminum polycrystalline	Electron diff.	Assumed normal		104

[a] No dislocation motion observed for films thinner than 500 A.

Nickel presents conflicting results. D'Antonio *et al.* report values for evaporated polycrystalline films that differ from the bulk value of 2.0×10^{12} dynes/cm^2 by only a few per cent. On the other hand, Jovanovic and Smith have found low values of the modulus for electroplated and chemically deposited films. Their chemical deposits containing 7 to 10% phosphorus are amorphous, or show at least a diffuse diffraction pattern. Figure 25 reproduces the stress-strain curves for cold-rolled foil, and electroplated and chemically deposited films several microns thick. The modulus $E/1 - v$ is about 2.0 for the chemical deposits, 2.3 for electrodeposits, 2.8 to 3.0 for rolled foils, and 3.0 for annealed bulk material (in units of 10^{12} dynes/cm^2). Upon heat treating the chemical deposits the modulus increases somewhat, but the deposits still

remain brittle. Yamamoto (*110*) found large changes in Young's modulus for
nickel films electrodeposited on copper substrates when the pH value of the
plating bath was varied (*109*).

With only few exceptions, the experiments indicate that no abnormal elastic
modulus is found in films, and we shall adopt this point of view. Present
theory, in any case, does not offer any mechanism which might generate large
changes of the elastic modulus. The low modulus of chemical nickel deposits
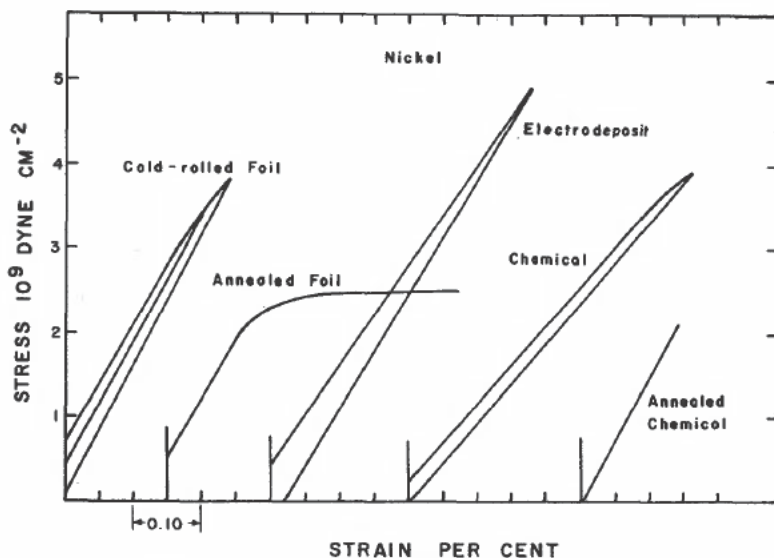
Fig. 25. Stress-strain curves for nickel films prepared in different ways. [After Jovanovic
and Smith (*91*).]

probably can be explained by the co-deposition of phosphorus from the bath.
Conventional theory might thus be used for calculating the elastic constants
of films.

b. Plasticity. Creep has been observed in almost every stress study of films.
Figure 26 shows some data by Oding and Aleksanyan. The discontinuous
nature of this creep curve also appears in the stress-strain curves published
by these authors. Since these results have not been duplicated by other work-
ers, they are somewhat suspect and might have been caused by their rather
rudimentary tensile machine.

According to Neugebauer, more precise measurements yield a creep rate
for gold which varies from 10^{-7} to 10^{-4}/min, depending on load, dimensions,
and amount of prestraining (*94*). Catlin and Walker (*90*) have observed a
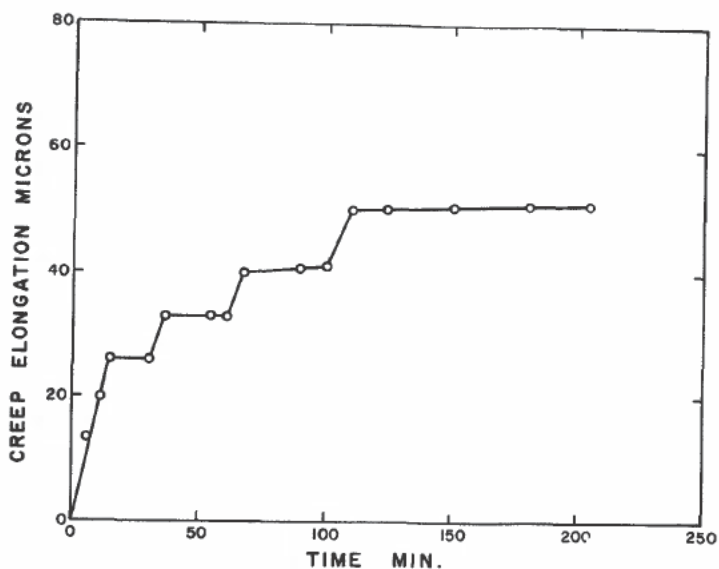
FIG. 26. Creep curve for copper film under load of 34 kg/mm². [After Oding and Aleksanyan (96).]
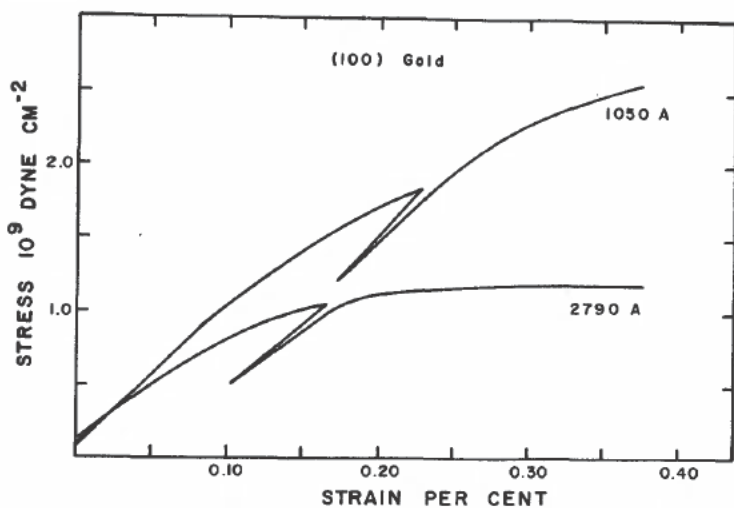
FIG. 27. Stress-strain curves of (100) gold films for two thicknesses. [Data from Catlin and Walker (90).]

short-time creep of gold films corresponding to a strain of about 5×10^{-5} in 15 sec. The stress-strain curve obtained by Catlin and Walker shows large amounts of plastic deformation and work hardening at higher strains (Fig. 27). Twinning was observed optically. A few small bands were formed at low stresses, but a large number of small bands appeared suddenly just below the ultimate tensile strength. In the thicker films these small bands grouped into one or more large bands with a laminated fine structure. The nonlinearity of the curve at low strains is partly caused by the smoothing of film wrinkles generated by the differential thermal expansion between film and substrate, but the behavior at higher strains is felt to be representative of the film itself.

Pashley (*111*) has observed a slow motion of screw dislocations in (111) gold films of 200-A thickness. He also saw a faster motion confined to one slip plane, and single and multiple cross slips. In addition, he found a sudden splitting of a dislocation into two partials separated by a very wide ribbon of stacking faults, apparently caused by the pinning of the partials at the surface and by the stress due to the surface contamination layer. In annealed films, he noted low-angle boundaries and dislocation arrays. Pashley showed in a later paper (*103*) that the extension is completely elastic at fracture in (111) gold films thinner than 500 A. Thicker films exhibited plastic behavior, but this was confined to regions of localized thinning in the specimen. Palatnik *et al.* (*112*) measured the elastic strain in Al and Ag films by electron diffraction and found at fracture a maximum elastic deformation of 0.5 and 0.3%, respectively, as well as evidence for an initial compressive stress in Al.

The estimates of the relative elastic and plastic extension at fracture vary from completely elastic to about three-quarters for elastic gold, with the total strain about 0.8 to 1.2% at breaking. For nickel, elastic strains of about 0.85% and plastic strains of 0.67% were noted at fracture. Total strains of 2% have been found in copper. The plastic region for polycrystalline gold is significantly less than for single-crystal gold films. Most workers agree, however, that no easy glide region is found, that creep and plastic deformation take place even at low strains, and that the total elongation at fracture is usually 1 to 2% and exhibits a large elastic component. The deformation processes are similar in both single-crystal and polycrystal samples. Figure 28 shows a schematic representation of the difference according to Blakely (*17*).

A notably different behavior has been reported for an unconstrained single-crystal gold film which had been annealed for 3 hours at 1000°C in air (*17*). This film was considerably softer and more ductile, and it exhibited a total strain at fracture of about 10%. Such specimens show a decided "necking" near the center.

c. Fracture. Menter and Pashley (*100*) have reviewed the fracture mechanism of gold single-crystal films in detail. In this case, the mechanism of fracture is one of localized plastic deformation with a resultant thinning of the

R. W. HOFFMAN
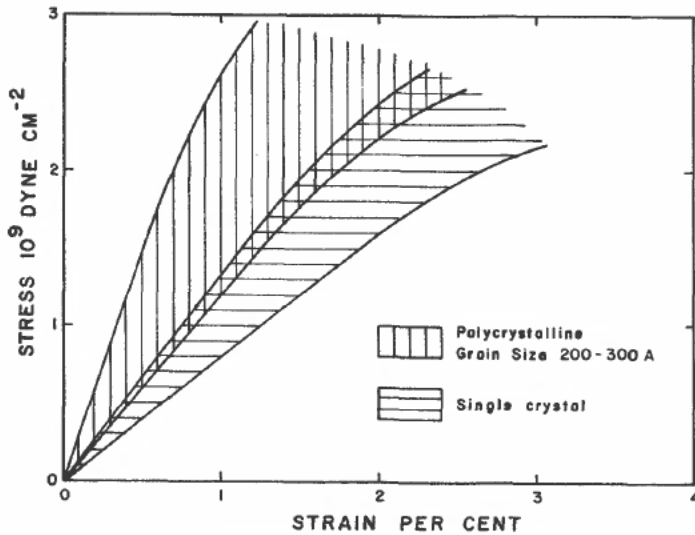
FIG. 28. Comparison of tensile behavior for polycrystalline and single-crystal gold films. The graph indicates representative results only. [After Blakely (17).]
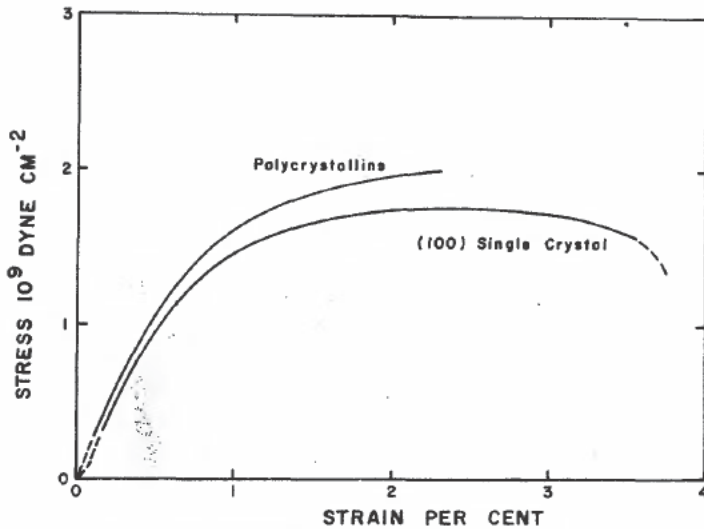
FIG. 29. Typical stress-strain curve for polycrystalline and single-crystal gold films at constant strain rate of 0.2% per minute. [Data from Blakely (17).]

film and a rise in the stress level. Eventually the smaller craks formed in this manner join, and the film fails. The dislocations responsible for the deformation are not the grown-in dislocations, but those which nucleate and multiply in discontinuous regions. They move on their glide planes until sufficient shear takes place to open the small cracks. Extensive piled-up groups of dislocations found after fracture indicate the generation of new dislocations as an important feature of the fracture process. Most observations show no necking just prior to fracture (94), but Blakely has found a low work-hardening region before fracture, and some evidence for necking in the decrease of the (nominal) flow stress (Fig. 29). The maximum stress seems to correspond to the stress needed to propagate cracks from flaws existing in the specimen. For polycrystalline nickel, a "clean-cleavage" type of fracture results (95).

 d. Tensile Strength. Much interest has been focused on the relatively high strength of films measured by various laboratories. The strengths are up to 200 times larger than those of annealed bulk samples, and they exceed the handbook values for hard-drawn material by a factor of 3 to 10. Available data are collected in Table VI; tensile strengths are quoted numerically and as fractions of the shear modulus. A thickness dependence of the strength has been reported by some and not found by others. Values quoted for the strength are maximum values of the breaking force divided by the original cross-sectional area, and presumably reflect the values for films without gross defects. All experimenters report a large scatter in their results.

 The main point of controversy is whether the ultimate tensile strength is a function of film thickness. Neugebauer (2) indicates that thickness dependence is found only with the bulge test, but D'Antonio et al. (95) (nickel) and Oding and Aleksanyan (96) (copper) have found a variation with thickness when using tensile machines. In experiments with silver, gold, and nickel films showing a variation of tensile strength with thickness, a large increase in strength is found below about 2000 A. At larger thicknesses the strength is about the same as that of heavily worked bulk material (Fig. 30). Films showing no thickness dependence have a strength about twice as great.

 Pashley (103), as well as Neugebauer (94), found for gold films a thickness-independent tensile strength in the range 500 to 12,500 A. The average strength observed was 40 kg/mm^2, but values from 20 to 80 kg/mm^2 were measured. The breaking strength was about the same for all film orientations, but polycrystalline films were slightly stronger than epitaxial single-crystal films. Blakely (17) made similar observations, but Catlin and Walker (90) found with the bulge method a pronounced thickness dependence of the ultimate tensile strength for (100) gold films. The tensile strength fell roughly linearly with increasing thickness over the narrow thickness range reported.

 Palatnik and Il'inskii (101) have measured the tensile strength in thick (20 to 150 μ) copper films. They report no thickness dependence, but find a decrease

TABLE VI

STRENGTH PROPERTIES

Material	Structure	Maximum tensile strength 10^9 dynes/cm^2	Shear modulus[a]	Strain at fracture, %	Thickness-dependent	Ref.
Au	Bulk hard-drawn	25[b]	G/114	—[c]	—	—
	(111) crystal film	79	G/36	1.2	No	100
	(100) crystal film	26	G/110	0.5	Yes	90
	(100) (111) polycrystalline film	48	G/59	1	No	94
	Polycrystalline film	53	G/54	0.7	Yes	89
	(100) crystal film	25	G/115	3.5	No	17
	Polycrystalline film	31	G/92	2.3	No	17
Ag	Bulk hard-drawn	36[b]	G/75	—	—	—
	Polycrystalline film	57	G/47	0.7	Yes	89
	Polycrystalline film	40	G/68	0.3–0.4	—	104
Cu	Bulk hard-drawn	47[b]	G/98	—	—	—
	Polycrystalline film	90	G/51	1.8	Yes	96
	Polycrystalline film	85	G/54	—	No	101
	Rolled foil	18	G/256	10–15	No	109
Ni	Bulk cold-rolled	120[b]	G/67	—	—	—
	Polycrystalline film	200	G/40	1.8	Yes	95
Al	Bulk cold-rolled	15[b]	G/171	—	—	—
	Polycrystalline film	40	G/66	0.5–0.8	Yes	104

[a] Shear moduli from "AIP Handbook," 1957.
[b] Bulk tensile strength from "Handbook of Chemistry and Physics," 42nd ed., 1961.
[c] Fracture strain not quoted for bulk material.

in strength with increasing deposition temperature (Fig. 31). Oding and
Aleksanyan (96) observed a thickness dependence on evaporated copper
films thinner than 4μ, but their electroplated copper films exhibited
constant strength.

In summary it can be said that the experimental data are not yet sufficient
to decide whether the strength of a thin film is usually thickness-dependent
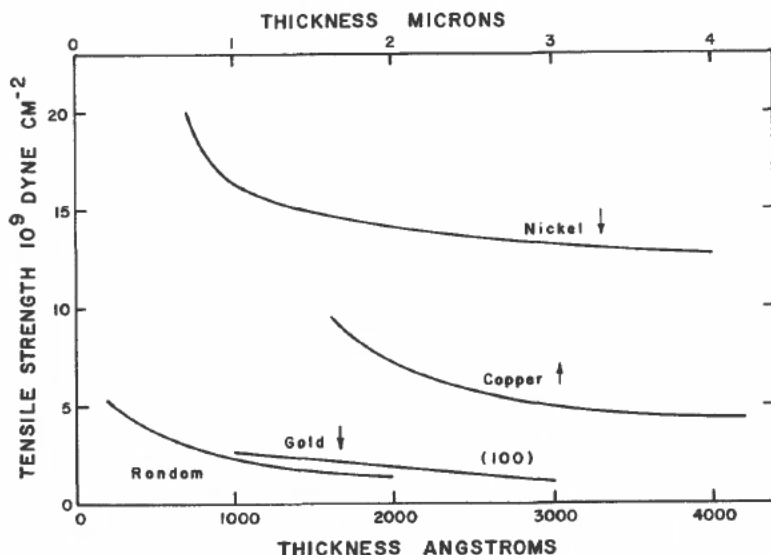
FIG. 30. Thickness dependence of tensile strength. For the nickel data (95) and gold
(89, 90) use the lower thickness scale; the copper data (96) are plotted on the upper thickness
scale.

or not. No common feature of material, orientation, or type of test seems to
correlate with the two types of behavior, and it may be that two forms of
strength behavior exist in grown films, depending on some as-yet-undetected
feature in the structure.

e. *Microhardness.* The only microhardness results found in the literature
were obtained on thick copper films (101, 112). Figure 31 reproduces the
observed microhardness and tensile strength as functions of the deposition
temperature. In the cited publications, the crystallite size and the microstrain
were determined from X-ray data. The scatter in microhardness (10%) was
about half the tensile-strength scatter. The authors found a strong correlation
of microhardness with strength.
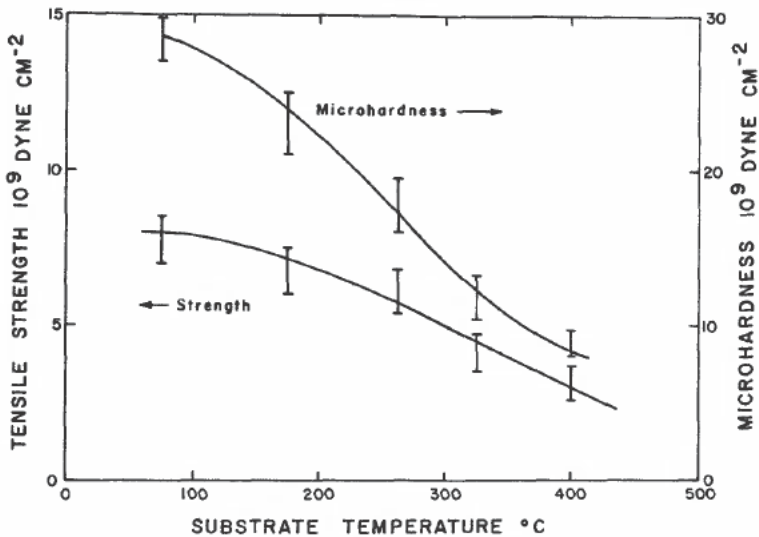
FIG. 31. Strength and microhardness of thick copper films as a function of substrate temperature during deposition. [After Palatnik and Il'inskii (*101*).]

3. MODELS FOR STRENGTH

The tensile properties of films, as we have seen, differ from the usual bulk properties. According to Menter and Pashley (*100*), the strength results from the film-deposition process, since foils thinned down from bulk specimens do not show the high strength associated with condensed films. The similarity of films and heavily cold worked metals, as well as the dissimilarity of films and whiskers, has been mentioned by Neugebauer (*94*). It is well known that the dislocation density in films is of the order of 10^{10} to $10^{12}/cm^2$, while cold-worked bulk material exhibits about two orders of magnitude less.

More precisely, we are led to the conclusion that the strength results from the absence of operating dislocation sources and restraining the motion of grown-in dislocations. Only when both mechanisms work together can high-strength films be expected. We shall treat briefly the influence of impurities, grain size, surface tension, other surface effects, and dislocation pinning on the strength of films. The impurity levels in the films tested thus far are not well known. However, precipitation hardening or internal oxidation have not been suggested as major strength contributions, and precipitates, in any case, have so far not been observed in films.

a. Grain Size. Grain-size effects on the yield stress of bulk material have been reported for some time [see Cracknell and Petch (*113*), for example],

and they have been suggested as the source for the high strength in films (*112*, *114*). The fact that single-crystal films have almost the same strength suggests, however, that the grain-size effects are not the most important factor, although they contribute to the small difference observed between polycrystalline and single-crystal films. Interesting is a comparison of films with foils. Lawley and Schuster found for rolled copper foils a thickness-dependent yield stress about five times larger than bulk, but a tensile strength that is independent of thickness and equal to bulk. The stress-strain curve is similar to that of a bulk tensile specimen, showing work hardening and large plastic strains at fracture. The yield stress in the thickness range from 7 to 50 μ follows the form

$$\sigma_{\text{yield}} = \sigma_0 + K t^{-1/2} \tag{17}$$

where σ_0 is about 3 kg/mm^2 and $K = 0.21$. The thickness is given in millimeters. The authors suggest that σ_0 results from the pinning of surface sources rather than a restriction of the dislocation length. The (thickness)$^{-1/2}$ term arises from a modification of the usual Petch analysis, which replaces the average grain diameter by the film thickness. D'Antonio and Tarshis (*115*) found that they could fit their data on polycrystalline nickel films to Eq. (17), although their data fit equally well a t^{-1} form (*116*). The replacement of the grain size by the thickness in the Petch analysis is plausible, since the two are at least roughly related.

b. Surface Effects. The surface can influence the film strength in a number of ways. Machlin (*117*) has discussed for bulk materials how the strength might be increased by surface effects: (1) Since the surface forms a barrier to the motion of dislocations, the dislocations pile up and increase in density near the surface; (2) surface drag effects result from the formation of a new surface due to the motion of a screw dislocation which intersects the surface; (3) surface anchoring effects are caused by pitting or etching; and (4) changes in modulus, lattice parameter, etc., occur near the surface.

Of the four contributions listed above, the first is not expected to operate in films, since dislocations are not expected to travel in a direction perpendicular to the plane of the film. (Dislocations moving parallel to the film plane, however, have been observed to pile up in thinned foils.) The second and third mechanisms can pin dislocations at the film surface, and the applied stress to move them can be calculated from the observed curvature of the dislocation. In the case of the aluminum and stainless steel, these stresses correspond to flow stresses in the work-hardened material and would not be large enough to account for the increased strength of films or their large elastic strain (*100*). The fourth contribution would be the film analogy to a fiber-reinforced material, but it is expected to be small for thin oxide layers and could not account for the strength of certain metal films.

Part of the strength of films may arise from their relatively perfect surface on a microscopic scale. Bilby (*118*) has shown that the energy to nucleate a dislocation at a perfect surface is so high that the process will not take place. A good surface will thus prevent nucleation in the thinner films, where sources can not operate. It has also been shown for fibers that they are only strong if the surface is undamaged (*119*).

Beams has calculated the compressive stress in a continuous film arising from surface tension and concludes that an appreciable increase in strength should result only at thicknesses less than about 100 to 200 A; this mechanism can therefore not account for the high strength observed on considerably thicker films.

c. Dislocation Pinning. Although one or more of the surface effects mentioned may contribute to the increased film strength, they do not seem large enough to explain the observed results. One must thus conclude that the pinned length of dislocations must be much smaller than the film thickness. As several investigators have pointed out, a number of different dislocation locking mechanisms can be conceived, as for instance: (1) pinning by point defects or impurities (2) pinning by jog formation after vacancy condensation, (3) severe tangling, and (4) effects due to stacking faults or twins. Unfortunately few details are known about the actual dislocation configurations and pinning modes in thin films, and a quantitative theory is lacking.

In assuming appreciably plastic deformation and a corresponding activation of dislocation sources, Blakely (*17*) finds an obstacle spacing of some 1500 A in gold films. Oding and Aleksanyan (*96*) deduct from the discontinuous nature of the stress-strain curve a periodic unloading of groups of dislocations which accumulate at obstacles. The discontinuous stress-strain curve might, however, result from static friction in the gravity-loaded system used, since no one else has observed discontinuous stress-strain curves in films.

Pashley (*103*) reports for gold samples that no dislocations parallel to the plane of the film are observed, and that the dislocations formed during the growth tend to be as short as possible and are randomly distributed throughout the film area. Since no tangles or regions of extremely high dislocation concentration were seen, one is tempted to rule out explanation (3) above.

Menter and Pashley (*100*) consider that the large elastic region observed on films arises from the contribution of the point defects. There is also some evidence derived from annealing kinetics that point defects may be present in large quantities in evaporated films (*75*).

We shall now turn to the question of sources. Dislocation network have been observed in thicker (>2000 A) evaporated gold films (*111*), and Menter and Pashley have outlined the mechanism of both single- and double-ended sources that may operate in thin films. No such sources have been observed, however. It is not expected that the Frank-Read source occurs in thin films,

but Wilsdorf (*120*) has found this source in thicker stainless-steel foils. He has also observed that grain boundaries, twin boundaries, and precipitates are good generators of dislocations. Nucleation of dislocations in the interior has been treated earlier. It is commonly assumed that point defects are the main contribution to the locking of dislocations, and at present it is still difficult to be more detailed than that.

d. Thickness Dependence. Of the mechanisms proposed, several have a built-in thickness variation and could account for the experiments that show such an effect. As commented earlier, surface-tension contributions would be larger the thinner the film, but should be important only in films thinner than 200 A. Beams has emphasized that the force to overcome the dislocation-line tension is larger for a smaller length, and on this basis, one should expect a thickness dependence of the strength even for a single-crystal film. For poly-crystalline films, the effect should be even more pronounced, as the lateral grain size will play a similar role.

The size dependence of fiber strength has also been attributed to the difficulty of making large fibers with good surfaces, and it appears that one finds no dependence of the strength on size if the fibers have really a smooth surface. It is possible that the thickness dependence of the film strength observed by some workers arises in a similar manner. An oxidized film surface with a different modulus, for instance, will cause such a thickness dependence, at least for films of modest thickness.

In analogy with the electrical resistivity of films, D'Antonio and Tarshis (*116*), have proposed that the strength should be expressed as the sum of terms arising from bulk behavior, imperfections, and a thickness effect,

$$\sigma_{total} = \sigma_{bulk} + \sigma_{imperfection} + \sigma_{thickness}$$

where σ_{bulk} represents the value for annealed material, $\sigma_{imperfection}$ the additional strength arising from the formation of the film and especially from the pinning of dislocations, and $\sigma_{thickness}$ a term accounting for the inhomogeneous features of the film and the surface effects. Following the approximate treatments of the electrical resistivity, one obtains an expression of the form

$$\sigma_{total} = \sigma_B\left(1 + \frac{K}{t}\right)$$

where σ_B is the bulk strength corresponding to the same lattice-defect structure as exhibited by the film, and K is a constant taking into account that dislocation motion changes with thickness. D'Antonio and Tarshis find a good fit to this expression for 750- to 4000-A-thick nickel films. As was mentioned earlier, however, one obtains an equally good fit if the same data are plotted according to Petch against $t^{1/2}$. (A recent paper by Grunes *et al.* (*121*)

shows the Petch form is more appropriate. Little plastic strain in both as deposited and annealed films was noted. It is suggested the strength arises from the high defect density and the proximity of the surfaces.)

We see that neither the tensile properties nor the internal stresses are really well understood. The problem is caused to a large degree by the wide variety of results published by different laboratories. Although most features can be "explained" qualitatively, it is this scatter of experimental data which makes it difficult to test general theories of film strength and stresses. Much remains to be done before the mechanical properties of condensed films can be predicted with some accuracy.

REFERENCES

1. R. E. Thun, in "Physics of Thin Films" (G. Hass, ed.), Vol. 1, p. 187. Academic Press, New York, 1963.
2. C. A. Neugebauer, in "Physics of Thin Films" (G. Hass and R. E. Thun, eds.), Vol .2. Academic Press, New York, 1964.
3. D. Walton, J. Chem. Phys. 37, 2182 (1962).
4. G. A. Bassett, J. W. Menter, and D. W. Pashley, in "Structure and Properties of Thin Films" (C. A. Neugebauer, J. D. Newkirk, and D. A. Vermilyea, eds.), p. 111. Wiley, New York, 1959.
5. A. E. Curzon, private communication.
6. D. W. Pashley, M. J. Stowell, M. H. Jacobs, and T. J. Law, Phil. Mag. 10, 127 (1964).
7. G. A. Bassett, Proc. European Regional Conf. Electron Microscopy Delft 1960, 270.
8. D. W. Pashley, in "Thin Films" (Wilsdorf, ed.), p. 59. American Society for Metals, Cleveland, Ohio, 1964.
9. R. H. Jeppesen and H. L. Caswell, IBM J. Res. Develop. 7, 297 (1963).
10. W. E. Vesely and R. W. Hoffman, B. S. Thesis, Case Institute of Technology, Cleveland, Ohio, 1964.
10a. E. L. Lee, P. E. Bolduc, and C. E. Violet, Phys. Rev. Letters B, 800 (1964).

11. D. O. Smith, M. S. Cohen, and G. P. Weiss, J. Appl. Phys. 31, 1755 (1960).
12. E. W. Pugh, E. L. Boyd, and J. F. Freedman, IBM J. Res. Develop. 4, 163 (1960).
13. D. O. Smith, E. E. Huber, Jr., M. S. Cohen, and G. P. Weiss, J. Appl. Phys. 31, 295S (1960).
14. S. G. Fleet, Mullard Res. Lab. Rep. 466, 1963.
15. D. S. Campbell, D. J. Stirland, and H. Blackburn, Phil. Mag. 7, 1099 (1962).
16. R. S. Sennett and G. D. Scott, J. Opt. Soc. Am. 40, 203 (1950).

17. J. M. Blakely, *J. Appl. Phys.* **35**, 1756 (1964).
18. L. S. Palatnik, M. Ya.Fuks, B. T. Boiko, and V. B. Pariiskii, *Fiz. Metal. i Metalloved.* **11**, 864 (1961); *Phys. Metal Metallog.(USSR) English Transl.* **11**(6), 44 (1961).
19. H. Hu, *in* "Electron Microscopy and Strength of Crystals" (G. Thomas and J. Washburn, eds.), p. 535. Wiley (Interscience), New York, 1963.
19a. M. L. Gimpl, A. D. McMaster, and N. Fuschillo, *J. Appl. Phys.* **35**, 3572 (1964).
19b. L. Bachmann, D. L. Sawyer, and B. M. Siegel, *J. Appl. Phys.* **36**, 304 (1965).
20. D. M. Evans and H. Wilman, *Acta Cryst.* **5**, 731 (1952).
21. M. H. Jacobs and D. W. Pashley, *Electron Microscopy Proc. Cambridge Conf.* 1963.
22. G. R. Booker, *Electron Microscopy Proc. Cambridge Conf.* 1963.
23. D. W. Pashley and A. E. B. Presland, *Proc. European Conf. Regional Electron Microscopy Delft* 1960, 391 (1960).
24. O. Beeck, A. E. Smith, and A. Wheeler, *Proc. Roy. Soc. (London)* A177, 62 (1964).
25. J. A. Allen, C. C. Evans, and J. W. Mitchell, *in* "Structure and Properties of Thin Films" (C. A. Neugebauer, J. D. Newkirk, and D. A. Vermilyea, eds.), p. 46. Wiley, New York, 1959.
26. G. G. Stoney, *Proc. Roy. Soc. (London)* A82, 172 (1909).
27. H. P. Murbach and H. Wilman, *Proc. Phys. Soc. (London)* B66, 911 (1953).
28. A. F. Turner, "Thick Thin Films," Tech. Rept. Bausch and Lomb, Rochester, New York, 1951.
29. E. C. Crittenden, Jr. and R. W. Hoffman, *Phys. Rev.* **78**, 349 (1950).
30. H. Blackburn and D. S. Campbell, *in* "Eighth National Symposium on Vacuum Technology Transactions, p. 943. Pergamon Press, New York, 1961.
31. H. Blackburn and D. S. Campbell, *Phil. Mag.* **8**, 823 (1963).
32. H. S. Story and R. W. Hoffman, *Proc. Phys. Soc. (London)* B70, 950 (1957).
32a. E. Klokholm *IBM Res. Rept. RC 1352* (1965).
33. J. R. Priest and H. L. Caswell, *in* "Eighth National Symposium Vacuum Technology Transactions," p. 947. Pergamon Press, New York, 1961.
34. J. D. Finegan and R. W. Hoffman, *J. Appl. Phys.* **30**, 597 (1959).
35. A. Kinbara, *Oyo Butsuri* **30**, 391 (1961).
36. J. Priest, H. L. Caswell, and Y. Budo, *J. Appl. Phys.* **34**, 347 (1963).
37. A. Brenner and S. Senderoff, *J. Res. Natl. Bur. Stand.* **42**, 105 (1949).
38. J. D. Finegan, *AEC Tech. Rept. 15*, Case Institute of Technology, Cleveland, Ohio, 1961.
39. S. P. Timoshenko, *Mech. Eng.* 259 (1923).
40. N. N. Davidenkov, *Soviet Phys.-Solid State English Transl.* **2**, 2595 (1961).
41. J. D. Finegan and R. W. Hoffman, *in* "Eighth National Symposium on Vacuum Technology Transactions," p. 935. Pergamon Press, New York, 1961.
42. Charles S. Smith, private communication.
42a. R. Glang, R. A. Holmwood, and R. L. Rosenfeld, *Rev. Sci. Instr.* **36**, 7 (1965).
42b. D. J. Dumin, *J. Appl. Phys.* **36**, 2700 (1965).
43. H. Horikoshi and N. Tamura, *J. Appl. Phys. Japan* **2**, 328 (1963).
44. J. D. Finegan and R. W. Hoffman, *AEC Tech. Rept. 18*, Case Institute of Technology, Cleveland, Ohio, 1961.
45. A. Kinbara, *Oyo Butsuri* **30**, 496 (1961).
46. A. Kinbara and H. Haraki, *J. Appl. Phys. Japan* **4**, 243 (1965).
47. J. S. Halliday, T. B. Rymer, and K. H. R. Wright, *Proc. Roy. Soc. (London)* A225, 548 (1954).
48. J. F. Freedman, *IBM J. Res. Develop.* **6**, 449 (1962).
48a. R. W. Vook and F. Witt, *J. Appl. Phys.* **36**, 2169 (1965).

49. J. R. MacDonald, *Phys. Rev.* **106**, 890 (1957).
50. R. H. Blumberg and D. P. Seraphim, *J. Appl. Phys.* **33**, 163 (1962).
50a. J. N. Zemel, N.A.T.O. Summer School on Thin Films, London (1965).
51. G. P. Weiss and D. O. Smith, *J. Appl. Phys.* **33**, 1166S (1962).
52. E. Klokholm, *IBM Res. Rept. RC 1508* (1965).
53. J. Riesenfeld and R. W. Hoffman, *AEC Tech. Rept. 39*, Case Institute of Technology, Cleveland, Ohio, 1965.
54. H. Kato, K. Nagasima, and H. Hasunuma, *Oyo Butsuri* **30**, 700 (1961).
55. H. Horikoshi, Y. Ozawa, and H. Hasunuma, *J. Appl. Phys. Japan* **1**, 304 (1962).
56. K. Kinosita, H. Kondo, and I. Sawamuru, *J. Phys. Soc. Japan* **15**, 942 (1960).
57. Y. Doi, *Machine Testing Laboratory Report (Japan)* **27**, 44 (1958).
58. M. Prutton, *Nature* **193**, 565 (1963).
59. H. Kondo and K. Kinosita, *Oyo Butsuri* **28**, 553 (1959).
60. O. S. Heavens and S. D. Smith, *J. Opt. Soc. Am.* **47**, 469 (1957).
60a. A. E. Ennos, *Appl. Opt.* **5**, 51 (1966).
60b. K. Kinosita, K. Nakamizo, K. Maki, K. Onuki, and K. Takeuchi, *J. Appl. Phys. (Japan)* **45**, 340 (1965).
61. J. Priest, H. L. Caswell, and Y. Budo, *Vacuum* **12**, 301 (1962).
62. J. E. Davey and R. H. Deiter, *J. Appl. Phys.* **36**, 284 (1965).
63. R. W. Hoffman, R. D. Daniels, and E. C. Crittenden, *Proc. Phys. Soc. (London)* **B67**, 497 (1954).
64. A. M. Toxen, *Phys. Rev.* **123**, 442 (1961).
65. H. L. Caswell, J. R. Priest, and Y. Budo, *J. Appl. Phys.* **34**, 3261 (1963).
66. W. C. Ellis, D. F. Gibbons, and R. G. Treuting, *in* "Growth and Perfection of Crystals" (R. H. Doremus, B. W. Roberts, and D. Turnbull, eds.), p. 102. Wiley, New York, 1958.
67. J. Riesenfeld and R. W. Hoffman, *AEC Tech. Rept. 32*, Case Institute of Technology, Cleveland, Ohio, 1964.
68. J. H. Van der Merwe, *Phil. Mag.* **7**, 1433 (1962).
69. J. H. Van der Merwe, *J. Appl. Phys.* **34**, 117 (1963).
70. J. H. Van der Merwe, *J. Appl. Phys.* **34**, 123 (1963).
71. J. H. Van der Merwe, *J. Appl. Phys.* **34**, 3420 (1963).
72. J. W. Matthews, *Phil. Mag.* **6**, 1347 (1961).
73. R. W. Hoffman, F. J. Anders, and E. C. Crittenden, Jr., *J. Appl. Phys.* **23**, 231 (1953).
74. R. W. Hoffman and H. S. Story, *J. Appl. Phys.* **27**, 193 (1956).
75. N. S. Rasor, *ONR Tech. Rept. 14*, Case Institute of Technology, Cleveland, Ohio, 1955.
76. H. G. Van Bueren, "Imperfections in Crystals," 2nd ed. North-Holland, Amsterdam, 1961.
77. H. D. Keith, *Proc. Phys. Soc. (London)* **B69**, 180 (1956).
78. T. B. Rymer, *Proc. Roy. Soc. (London)* **A225**, 274 (1956).
79. T. B. Rymer, F. J. Fayers, and S. J. Hewitt, *Proc. Phys. Soc. (London)* **B69**, 1059 (1956).
80. E. K. Halteman, *J. Appl. Phys.* **23**, 150 (1952).
81. R. Bacon, M.S. Thesis, Case Institute of Technology, Cleveland, Ohio, 1953.
82. R. S. Smith, *IBM J. Res. Develop.* **4**, 205 (1960).
83. A. Segmüller, *IBM J. Res. Develop.* **6**, 464 (1963).
84. A. Segmüller, *Z. Metallk.* **54**, 248 (1963).
85. T. B. Rymer, *Nuovo Cimento* **6**, 294 (1957).
86. W. Pitsch, *Arch. Eisenii Henwegen* **28**, 745 (1957).
86a. K.H. Behrndt, *J. Vac. Sci. Tech.* **2**, 63 (1965).

87. M. S. Cohen, E. E. Huber, Jr., G. P. Weiss, and D. O. Smith, *J. Appl. Phys.* **31**, 291S (1960).
88. J. W. Beams, J. B. Breazeale, and W. L. Bart, *Phys. Rev.* **100**, 1657 (1955).
89. J. W. Beams, *in* "Structure and Properties of Thin Films" (C. A. Neugebauer, J. D. Newkirk, and D. A. Vermilyea, eds.), p. 183. Wiley, New York, 1959.
90. A. Catlin and W. P. Walker, *J. Appl. Phys.* **31**, 2135 (1960).
91. S. Jovanovic and Cyril S. Smith, *J. Appl. Phys.* **32**, 121 (1961).
92. R. Papirno, *J. Appl. Phys.* **32**, 1175 (1962).
93. D. M. Marsh, *J. Sci. Instr.* **38**, 229 (1961).
94. C. A. Neugebauer, *J. Appl. Phys.* **31**, 1096 (1960).
95. C. D'Antonio, J. Hirschhorn, and L. Tarshis, *Trans. AIME* **227**, 1346 (1963).
96. A. Oding and I. T. Aleksanyan, *Soviet Phys.-Doklady English Transl.* **8**, 818 (1964).
97. D. Kuhlmann-Wilsdorf and K. S. Raghavan, *Rev. Sci. Instr.* **33**, 930 (1962).
98. A. Lawley and S. Schuster, *Rev. Sci. Instr.* **33**, 1178 (1962).
99. E. Orowan, *Z. Physik* **82**, 235 (1933).
100. J. W. Menter and D. W. Pashley, *in* "Structure and Properties of Thin Films" (C. A. Neugebauer, J. D. Newkirk, and D. A. Vermilyea, eds.), p. 111. Wiley, New York, 1959.
101. L. S. Palatnik and A. I. Il'inskii, *Soviet Phys.-Solid State English Transl.* **3**, 2053 (1962).
102. H. G. F. Wilsdorf, *Rev. Sci. Instr.* **29**, 323 (1958).
103. D. W. Pashley, *Proc. Roy. Soc. (London)* **A255**, 218 (1960).
104. L. S. Palatnik, M. Ya. Fuks, B. T. Boiko, and A. T. Pugacheu, *Soviet Phys.-Doklady English Transl.* **8**, 713 (1964).
105. R. W. Hoffman, *in* "Thin Films" (Wilsdorf, ed.), p. 99. American Society for Metals, Cleveland, Ohio, 1964.
106. G. A. Bassett and D. W. Pashley, *J. Inst. Metals* **87**, 449 (1959).
107. D. M. Marsh, *J. Sci. Instr.* **36**, 165 (1959).
108. J. E. Gordon, *in* "Growth and Perfection of Crystals" (R. H. Doremus, B. W. Roberts, and D. Turnbull, eds.), p. 219. Wiley, New York, 1958.
109. A. Lawley and S. Schuster (to be published in *Trans. AIME*).
110. Y. Yamamoto, *Tech. Rept. 2 of Kanazawa Univ. Japan*, 1954.
111. D. W. Pashley, *Phil. Mag.* **4**, 324 (1959).
112. L. S. Palatnik, G. V. Fedorov, and A. I. Il'inskii, *Fiz. Metal. i Metalloved.* **5**, 815 (1961). *Phys. Metals Metallog. (USSR) English Transl.* **5**, 159 (1961).
113. A. Cracknell and M. J. Petch, *Acta Met.* **3**, 186 (1955).
114. W. K. Ford, Ph.D. Thesis, University of Virginia, Charlottesville, Virginia, 1959.
115. L. Tarshis, private communication.
116. C. D'Antonio and L. Tarshis (to be published).
117. E. S. Machlin, *in* "Strengthening Mechanisms in Solids," p. 375. American Society for Metals, Cleveland, Ohio, 1960.
118. B. A. Bilby, Cambridge Conference on Mechanical Properties of Whiskers and Thin Films, reported in *Nature* **182**, 296 (1958).
119. D. M. Marsh, Royal Society Symposium on New Materials, London, 1963.
120. H. G. F. Wilsdorf, *in* "Structure and Properties of Thin Films" (C. A. Neugebauer, J. D. Newkirk, and D. A. Vermilyea, eds.), p. 515. Wiley, New York, 1959.
121. R. L. Grunes, C. D'Antonio, and F. Kies, *J. Appl. Phys.* **36**, 2735 (1965).